Seismic hazard maps based on Neo-deterministic Seismic Hazard Assessment for China Seismic Experimental Site and adjacent areas

Yan Zhang [a], Fabio Romanelli [b,d,*], Franco Vaccari [b], Antonella Peresan [c], Changsheng Jiang [a], Zhongliang Wu [d], Shanghua Gao [d], Vladimir G. Kossobokov [e,f], Giuliano F. Panza [a,f,g,h,i]

[a] Institute of Geophysics, China Earthquake Administration, Beijing, China
[b] Department of Mathematics and Geosciences, University of Trieste, via E. Weiss 4, 34128 Trieste, Italy
[c] National Institute of Oceanography and Applied Geophysics CRS-OGS, Udine, Italy
[d] Institute of Earthquake Forecasting, China Earthquake Administration, Beijing, China
[e] Institute of Earthquake Prediction Theory and Mathematical Geophysics, Russian Academy of Sciences, Moscow, Russia
[f] International Seismic Safety Organization, ISSO, Arsita, Italy
[g] Accademia Nazionale dei Lincei, Rome, Italy
[h] Accademia Nazionale delle Scienze detta dei XL, Rome, Italy
[i] Beijing University of Civil Engineering and Architecture (BUCEA), Beijing, China

ARTICLE INFO

Keywords:
China Seismic Experimental Site
Seismic hazard
NDSHA
Design ground acceleration
M_{design}

ABSTRACT

Many devastating earthquakes inflicted heavy casualties and property losses in the seismically active China Seismic Experimental Site area (CSES: 97.5° ~ 105.5°E, 21° ~ 32°N). We performed a first-order seismic zoning based on Neo-deterministic Seismic Hazard Assessment (NDSHA) in the study area delimited by 94° ~ 108°E and 19° ~ 35°N, containing the South-East margin of the Tibetan Plateau and the Sichuan-Yunnan region. The seismic hazard is expressed by maps of peak ground displacement (PGD), peak ground velocity (PGV) and design ground acceleration (DGA) values, extracted from synthetic seismograms computed at a regional scale and mapped on a regular grid of 0.2° × 0.2° over the study area. For the computation of synthetic seismograms, we considered and updated all the available geophysical-geological-tectonic information, including historical and instrumental earthquake catalogues, seismogenic zones, seismogenic nodes, focal mechanisms, and geophysical structural models. We tested the performance of our assessments with available data (i.e., after the Great Wenchuan (2008, May 12th, M_s = 8.0) and Lushan (2013, April 20th, M_s = 7.0) earthquakes) and verified the negligible influence of large events located "far" from the study area. The results indicate the high seismic hazard of the region, with a particular attention (i.e., where DGA > 0.6 g) to the areas located around the main fault zones, e.g., the Longmenshan, Anninghe and Zemuhe Fault Zones. These first-order NDSHA zoning findings may serve as a knowledge basis to support both large- to mid-range preparedness actions and (multi-scenario) site-specific studies.

1. Introduction

As a result of sustained economic growth and urbanization process in Asia, the increasing asset values and Gross Domestic Product (GDP) are exposed to natural hazards (e.g., Wu et al., 2017; Sarica et al., 2020). Seismic risk is generally qualitatively described by the following formula:

Risk = Hazard x Exposure x Vulnerability

This formula was first used in flood risk (e.g., Kron, 2002), and later commonly applied also to seismic risk analysis. **Risk** increases with increasing **Exposure**, even when **Hazard** and **Vulnerability** remain the same. Although **Hazard** is impossible to be under control, the irreversible trend of societal expansion directly increases **Exposure**, and finally makes **Risk** larger. Therefore, the most effective action is to decrease **Vulnerability**. It can be achieved by updating seismic codes and adopting better aseismic design, and also by deepening the understanding of seismic hazard level, i.e., obtaining a reliable and realistic estimation of seismic hazard and avoiding the construction of important infrastructures in areas with high hazard levels. In the 1960s, the

* Corresponding author at: Department of Mathematics and Geosciences, University of Trieste, via E. Weiss 4, 34128 Trieste, Italy.
E-mail address: romanel@units.it (F. Romanelli).

Accepted 24 May 2021

Probabilistic Seismic Hazard Assessment (PSHA) was first formalized (Cornell, 1968) and widely applied worldwide. However, as the first numerical approach for computing seismic hazard, PSHA has been constantly questioned and critiqued in recent years (e.g., Wyss et al., 2012; Panza and Bela, 2020 and references therein). The Neo-deterministic Seismic Hazard Assessment (NDSHA) was firstly introduced in 1996 (Panza et al., 1996) and has developed into a multi scenario- and physics-based methodology.

Since 1000 CE, nineteen large devastating earthquakes with $M \geq 7.5$, five with $M \geq 8.0$, have occurred in the South-East margin of the Tibetan Plateau and the Sichuan-Yunnan region (Fig. 1). These events mainly occurred along the Xianshuihe, Longmenshan, Anninghe, Zemuhu, and Xiaojiang Fault Zones. Among these events, the May 12th, 2008 $M_s = 8.0$ Wenchuan earthquake, the April 20th, 2013 $M_s = 7.0$ Lushan earthquake, the August 3rd, 2014 $M_s = 6.5$ Ludian earthquake, and the June 17th, 2019 $M_s = 5.7$ Changning earthquake invariably caused heavy casualties and property losses (Wu et al., 2019). For example, the 2008 $M_s = 8.0$ Wenchuan earthquake claimed 69,226 victims, with 17,923 people missing, 374,643 people injured, and economic losses as large as 845.1 billion yuan (RMB). It resulted in more than five million people becoming homeless and countless property losses, involving houses, schools, hospitals and other non-residential urban infrastructures (Chen and David, 2011). Facing such a severe threat, it is crucial and urgent to conduct a seismic hazard estimation considering all the available probabilistic and deterministic approaches. In China, the national Seismic Ground Motion Parameters Zonation Map of China (NSGMP), also referred to as GB18306 - 2015[1], is based on PSHA and has been updated to the 5th version (Gao and Tian, 2015). Wang et al. (2019) computed the probabilistic distribution of PGA > 0.15 g in the Sichuan-Yunnan region for the next 30 years. Ding et al. (2004) applied early NDSHA and obtained the first deterministic seismic hazard map in North China. However, In the seismically active Sichuan and Yunnan Provinces, seismic hazard maps produced by either deterministic or neo-deterministic seismic hazard approach are absent. In this study, following the application of NDSHA in other countries (e.g., India, see Parvez et al., 2003, 2017), we performed a first-order regional seismic hazard assessment using NDSHA, aiming to deepen the understanding of seismic hazard in the study area (Fig. 1), containing the South-East margin of the Tibetan Plateau and the Sichuan-Yunnan region.

1.1. China Seismic Experimental Site (CSES)

On 12 May 2018, at the opening ceremony of the International Conference for the Decade Memory of the Wenchuan Earthquake with the 4th International Conference on Continental Earthquakes (4th ICCE), the establishment of the China Seismic Experimental Site (CSES) in the Sichuan-Yunnan region was officially announced.[2, 3] The site is located in Southwest China, close to the eastern Himalayan syntaxes (EHS), covers the Sichuan and Yunnan Provinces, and the southeastern margin of the Tibetan Plateau. The long-term collision between the Eurasian and Indian plates resulted in complex geodynamic and tectonic environments in this area, one of the most representative features of which is the development of complex fault systems (e.g., Shen et al., 2005; Gan et al., 2007). The main active faults and fault zones are shown in Fig. 1. The Longmenshan Fault Zone consists of a series of active faults, including two faults corresponding to the May 12th, 2008 $M_s = 8.0$ Wenchuan earthquake, i.e., the Yingxiu-Beichuan Fault (also called Central Fault) and the Jiangyou-Guanxian Fault (also called Qianshan Fault) (e.g., Zhang et al., 2009). These fault systems delimit multiple tectonic blocks, such as the Chuandian (also called Sichuan-Yunnan), Qiangtang, Bayan-Har, and South-Yunnan Blocks. Most tectonic activity and earthquakes with $M \geq 7.5$ occurred along the boundaries of these active tectonic blocks (e.g., Zhang et al., 2003).

1.2. Why NDSHA?

Xu and Gao (2014) noted that the high uncertainties affecting the catalogues of historical destructive earthquakes were due to the incomplete documentation caused by damages from historical wars and natural hazards. The records for historical earthquakes span long-time scale, which are controlled by many factors, such as official documents, folk literature (Wen et al., 2008), and geological seismic investigations, e.g., the large historical earthquakes identified along the Chenghai Fault (Yang et al., 2020). Wen et al. (2008) systematically investigated the patterns and features of historical earthquakes in the Xianshuihe, Anninghe, Zemuhe and Xiaojiang Fault Zones. They found that the oldest earthquake in the Xianshuihe Fault Zone could be traced back to 1327 CE, in the Anninghe and Zemuhe Fault Zones could be traced back to 1480 CE, and in Xiaojiang Fault Zone could be traced back to 1500 CE. These observations may explain why the traceability of the occurrence time of historical earthquakes occurred in different fault zones is very inhomogeneous.

The catalogue of historical earthquakes (pre-1990) used in this study (Department of Earthquake Disaster Prevention, State Seismological Bureau, 1995) is shown in Fig. 2. The heterogeneous research and knowledge of historical earthquakes in different active fault/fault zones (Wen et al., 2008) and the high likelihood of overlooking possible earthquakes with occurrence rates longer than those detectable within accessible historical time scales, make it reasonable and acceptable to consider 1500 CE as the time after which historical earthquakes have been recorded with a completeness level satisfactory for the purposes of this study ($M_{completeness} = 5.0$). Another way to account for the possible occurrence of earthquakes with rates larger than those recordable within historical time scales is supplied by the introduction of seismogenic nodes (Gorshkov et al., 2003; Gvishiani et al., 2020 and references therein; Rugarli et al., 2019b), to be introduced in Section 3.3.

Fig. 3 shows that some clustering of the great earthquakes is likely to exist and accordingly, the definition of 'return period' for large earthquakes contradicts observations for them (e.g., Wen et al., 2008), and makes any attempt to estimate an "average return time" quite unrealistic and very uncertain (depending on the selected time span). Although hampered by the paucity of data, Chen et al. (2020) attempted to unravel the physical aspects of earthquakes occurrence. The features common to the catalogue CSESeventV2020 (to be introduced in Section 3.2) and to Chen et al. (2020) supply clear examples of the chimeric nature of 'return period' (i.e., periodic, characteristic event), and of Poissonian (i.e., memoryless) stationary earthquake occurrence. The inadequacy of the Poissonian model to derive hazard estimates from such a catalogue (regardless of its relation to incompleteness or to the intrinsic properties of earthquake time distribution) is evident, and demonstrates how hampered can be in any conclusion about the seismic hazard of the study area, based on standard PSHA procedure (e.g., McGuire, 2008; Stirling, 2014). These research findings represent a direct and mandatory motivation to use NDSHA, which does not require similar assumptions (for a recent review see Rugarli et al., 2019a, 2019b; Panza and Bela, 2020; Bela and Panza, 2021), while waiting for a more complete and deeper understanding of the physics of earthquakes.

2. Methodology

After being initiated in 1996 (Panza et al., 1996), and in response to several drawbacks of PSHA at the global level (e.g., Wyss et al., 2012), the NDSHA approach has undergone several iterations and improvements (e.g., Panza et al., 2001; Parvez et al., 2003; Peresan et al., 2011; Panza et al., 2012; Rugarli et al., 2019a; Panza and Bela, 2020; Bela and Panza, 2021). It has been developed as a comprehensive multi-disciplinary approach for performing scenario-based seismic hazard

[1] http://www.gb18306.net/. Last assessed on March 26, 2021.
[2] http://124.17.4.85/en/. Last accessed on March 2, 2021.
[3] http://www.cses.ac.cn/. Last accessed on March 26, 2021.

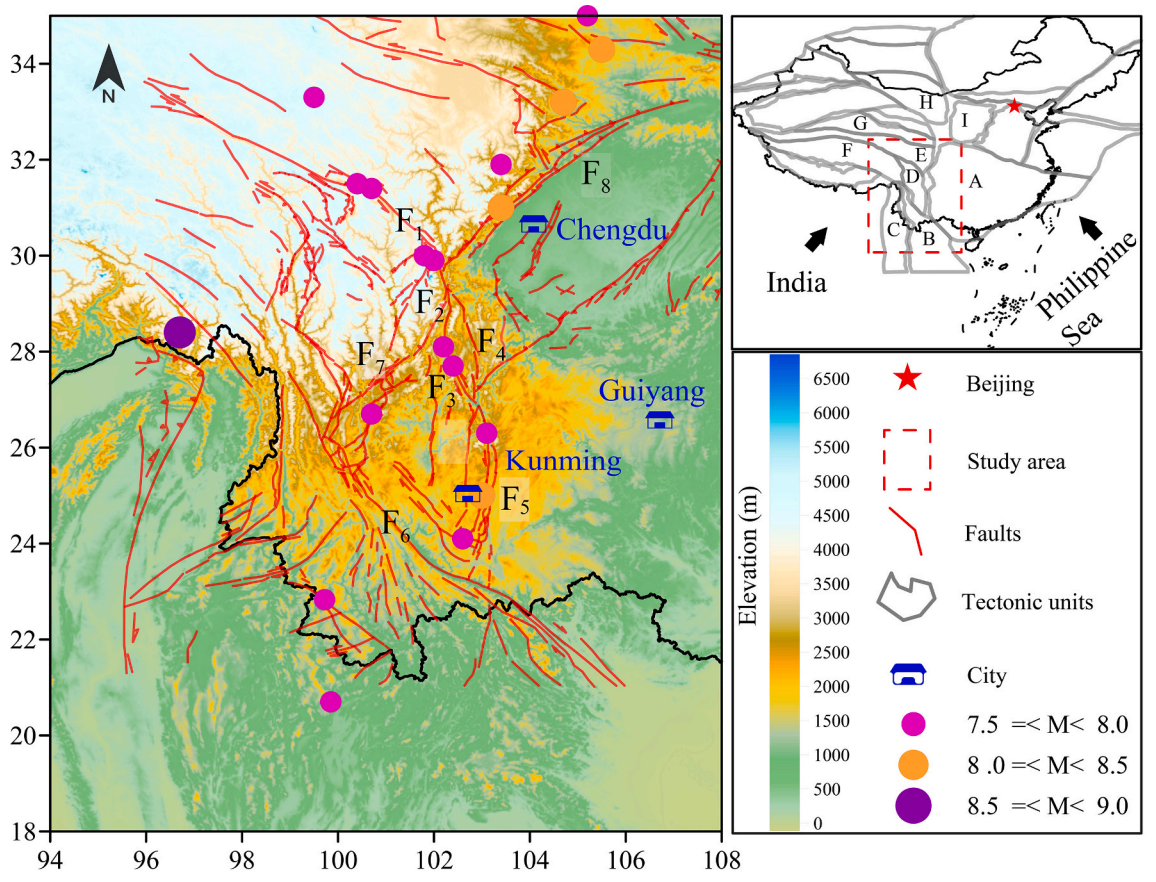

Fig. 1. The selected study area in this work (94° ~ 108°E, 18° ~ 35°N). Main active faults systems are marked by F_x (with x = 1,..,8): F_1, Xianshuihe Fault Zone; F_2, Anninghe Fault Zone; F_3, Zemuhe Fault Zone; F_4, Daliangshan Fault Zone; F_5, Xiaojiang Fault Zone; F_6, Honghe Fault Zone; F_7, Lijiang-Xiaojinhe Fault Zone; F_8, Longmenshan Fault Zone. Various colored circles show the spatial distribution of large earthquakes with $M \geq 7.5$ that occurred from 1000 to 2019 CE. Three blue building-shaped symbols indicate locations of Chengdu, Guiyang, and Kunming Cities. In the top-right subfigure, the red dotted box displays the respective location of the study area on mainland China. The two black arrows indicate the approximate moving direction of the India and the Philippine Sea plates. The size has no practical meaning. The irregular gray lines indicate the boundaries of different tectonic units, such as, A: South China Block, B: South Yunnan Block, C: West Yunnan Block, D: Chuandian (Sichuan-Yunnan) Block, E: Bayan-Har Block, F: Qiangtang Block, G: Qaidam Block, H: Alax Block, and I: Ordos Block. The red star indicates the location of Beijing City, the capital of China. The tectonic data is from Zhang et al. (2003). The earthquake catalogue is from the Department of Earthquake Disaster Prevention of China Earthquake Administration (1995), Department of Earthquake Disaster Prevention, China Earthquake Administration (1999) and the China Earthquake Networks Center (CENC). The fault data is from Deng et al. (2003). The elevation data is from https://www.ngdc.noaa.gov/mgg/global/ (Last accessed on March 2, 2021). (For interpretation of the references to colour in this figure legend, the reader is referred to the web version of this article.)

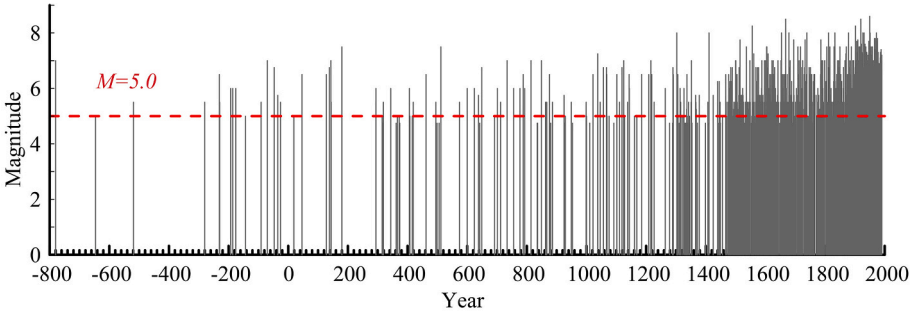

Fig. 2. Magnitude vs origin time of historical earthquakes (780 BCE ~ 1990 CE).

computations based on all available geophysical-geological-tectonic information. As a sustainable developing approach, NDSHA has been applied in many countries and regions, including Croatia (Markušić et al., 2000), northern Morocco (Vaccari et al., 2001), Egypt (El-Sayed et al., 2001), India (Parvez et al., 2003, 2017), North China (Ding et al., 2004), and North Africa (Mourabit et al., 2014). A detailed description of NDSHA has been provided in many published papers, such as Panza et al. (2001), Panza et al. (2012), Panza et al. (2013), Panza (2017), Rugarli et al. (2019a), and Panza and Bela (2020). Historical and instrumental earthquake catalogues, seismogenic nodes, seismogenic zones, focal mechanisms and regional polygons equipped with characteristic structural models are the five input datasets for standard NDSHA computations (Fig. 4). To enable processing using computers with limited computing power and resources, the efficient computation of

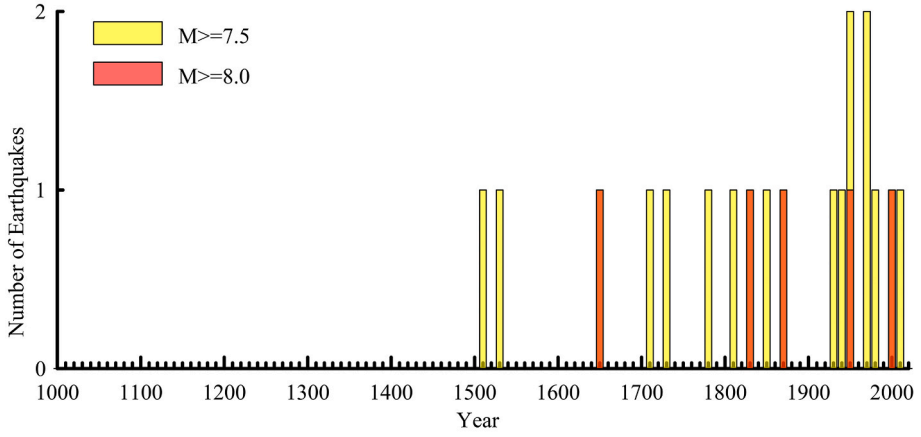

Fig. 3. Decadal number of large earthquakes, 1000 – 2019 CE. Red bars: $M \geq 8.0$; Yellow bars: $M \geq 7.5$. (For interpretation of the references to colour in this figure legend, the reader is referred to the web version of this article.)

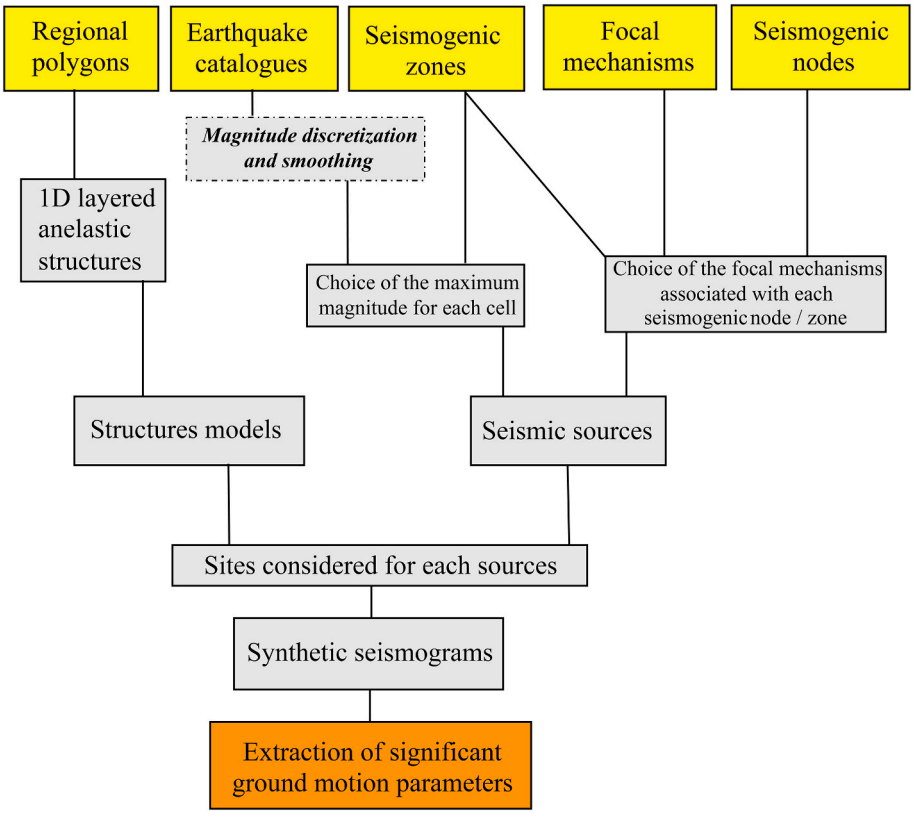

Fig. 4. Flow chart of the standard procedures of NDSHA, as briefly described in Section 2. Yellow boxes represent five different types of input datasets, namely, earthquake catalogues, seismogenic zones, focal mechanisms, seismogenic nodes and regional polygons with defined structural models. The outcomes of the procedures are in the orange rectangular box, which means the extraction of significant ground motion parameters from synthetic seismograms (i.e., PGD, PGV,and DGA). (For interpretation of the references to colour in this figure legend, the reader is referred to the web version of this article.)

reliable and realistic synthetic seismograms, i.e., the modal summation method (Panza, 1985; Florsch et al., 1991; Panza et al., 2001), was implemented in NDSHA. On account of the natural complexity and a lack of knowledge about the Earth's structure, regional polygons representing different structural models were defined based on available datasets (Zhang et al., 2014; Yao et al., 2019). Here, the study area was gridded with $0.2^\circ \times 0.2^\circ$ cells. The earthquake catalogue was discretized with the same gridding rule and then smoothed to account for the epicentral location error and for the finite dimension of seismic sources. The spatial coverage of smoothed seismicity was limited within the seismogenic zones, which limits the spatial range of potential damaging earthquake sources. Each seismogenic zone was assigned with a single characteristic focal mechanism according to the known focal mechanism datasets (focal mechanism catalogue of CSES[4] and GCMT[5]). The introduction of seismogenic nodes, which define the areas that are historically not yet active but prone to large earthquakes in the future, provided a significant supplement to earthquake catalogues. All the cellular sources defined were used in the computation of synthetic seismograms.

[4] http://www.ief.ac.cn/Community/info/2020/22555.html. Last accessed on September 11, 2020.
[5] https://www.globalcmt.org/. Last accessed on September 11, 2020.

3. Input data

NDSHA does not rely on any statistical models, but instead relies on the physical knowledges of the seismic sources, the pathways of seismic waves, and the site conditions. In this study, five types of input datasets were considered: (1) seismogenic zones limiting potential areas for earthquakes, (2) seismogenic nodes defining areas prone to large earthquakes, even if not active in historical time, (3) catalogues of both historical and instrumental earthquakes, (4) focal mechanisms representing average stress/strain level in each seismogenic zone, and (5) structural models taking into the account attenuation of propagating seismic waves.

3.1. Seismogenic zones

The NSGMP has been updated since 1957, and the latest version is the fifth-generation, released in 2015 (5NSGMP) (Gao and Tian, 2015). In the 5NSGMP, a total of 1206 seismogenic zones were determined based on a tri-class seismic source model containing seismic provinces, background seismicity zones and tectonic feature zones (Pan et al., 2013).

In the framework of 5NSGMP, more than 100 seismogenic zones were contained in the selected study area. Some seismogenic zones were merged to decrease the total number of seismogenic zones, according to the following criteria: (a) the boundaries of active tectonic blocks(e.g., Zhang et al., 2003), (b) seismogenic zones including the same fault (or fault segment), (c) seismogenic zones of unknown type close to a national border, and (d) neighboring zones having the similar elongation direction (see Fig. S1 in the Supplementary Material, where the seismogenic zone marked by 5 shown in the Fig. S1[right] was merged from the seismogenic zones marked by 5, 7, 9 and 13 shown in the Fig. S1 [left], based on the criterion (a), (b) and (d)). The outcome of the processes described above resulted in 99 seismogenic zones (Fig. 5).

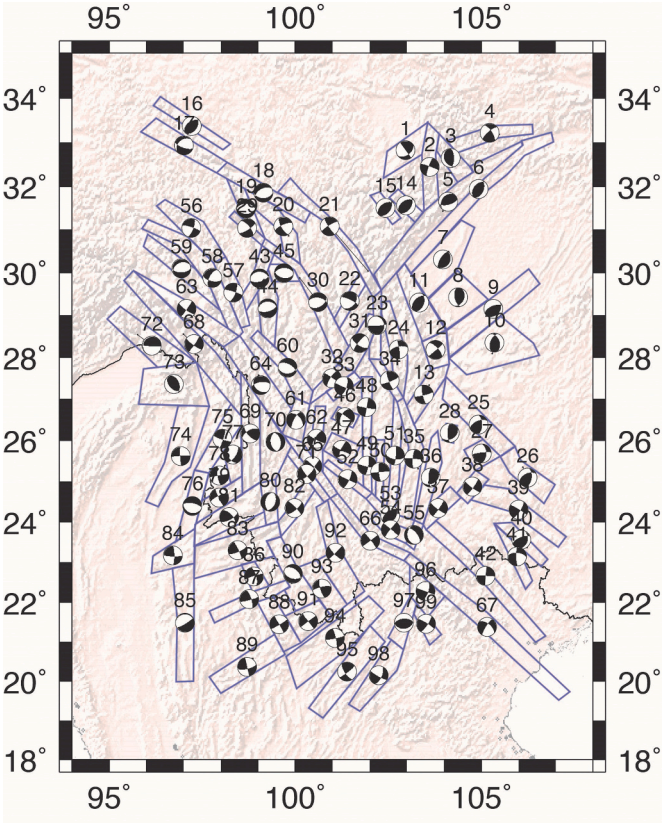

Fig. 5. The refined seismogenic zones and their representative focal mechanisms. More information about the unmerged seismogenic zones is shown in Fig. S1[left] of Supplementary Material.

3.2. Earthquake catalogues

The earthquake catalogue represents important information that describe the seismicity of the investigated area. According to Peresan and Ogwari (2010), an optimized catalogue CSESeventV2020 was assembled by properly integrating the two available old and new catalogues. The old catalogue spanning the time range from 780 BCE to 1990 CE was organized and digitized by the Department of Earthquake Disaster Prevention, China Earthquake Administration (1995); Department of Earthquake Disaster Prevention, China Earthquake Administration, 1999). The new catalogue spanning the time range from 1970 to 2019 was reported by the China Earthquake Networks Center (CENC). Cheng et al. (2017) proposed an M_W-based catalogue for mainland China, spanning the time range from 780 BCE to 2015 CE by unification of different magnitude types (M_S, M_W). However, according to Liu et al. (2017), it is unreasonable for the measured magnitude to be converted into another type. Therefore, in this study, we focused only on the values of magnitude, and the specific magnitude types were temporarily neglected.

The two catalogues have a time overlap of 20 years (1970 – 1990). For the period from 780 BCE to 1969 CE and the period from 1991 to 2019, straightforward merging was performed. For the period before 1900, i.e., 780 BCE to 1899 CE, 245 events were reported in the old catalogue, and because no seismic station recording was deployed to observe earthquakes that occurred before 1900, the magnitudes in this period were directly deduced from discrete intensity values. As illustrated in Fig. 2, the majority of the events in this period range from magnitude 5.0 to 8.0, and are characterized by a very sparse distribution before 1500. Accordingly, the earlier part of the old catalogue could only be tentatively considered complete for magnitude of 5.0 and above. For the 1900 – 1969 period, the catalogue can reasonably be considered complete for earthquakes with $M \geq 5.0$. For the 1970 – 1990 period, events recorded were prioritized in the new catalogue and, as a rule, we included in the CSESeventV2020 catalogue only the events from the old catalogue not reported in the new one. The optimized catalogue CSESeventV2020 contains 721,110 events for the time range from 780 BCE to 2019 CE. The gridded and smoothed distribution of CSESeventV2020 is shown in Fig. 6. As described in the right panel of Fig. 6, all epicenters were discretized into $0.2^\circ \times 0.2^\circ$ grid cells. In each cell, the maximum magnitude was retained. Epicenters were then smoothed with a radius of 3 cells to account for the source extension in space and the error of earthquake localizations (Panza et al., 1990). More details of the smoothing procedure can be found in Panza et al. (2001).

3.3. Seismogenic nodes

As a supplement to the seismicity reported in CSESeventV2020, the seismogenic nodes, namely the areas prone to strong earthquakes identified by pattern recognition applied to morphostructural analysis, helped to account for occurrence rates larger than those logged in the available catalogues.

The identification of those areas prone to strong earthquakes were performed by recognizing the intersections of morphostructural lineaments that separate mountain countries, mega-blocks, and blocks based on patterns of structures and landforms nearby, as described in Gvishiani et al. (2020). For each node, a circle (vicinities of lineament intersection) was used to define the possible spatial range of strong earthquakes, i.e., the target of the pattern recognition. In order to obtain an "upper bound estimate" for the potential magnitude in each node, it is necessary to define a M_{design}, which indicates the physically possible largest magnitude of the scenario event consistent with the values of magnitude observed or estimated by pattern recognition. Indeed, M_{design} defines the magnitude of Maximum Credible Earthquake (MCE) (Rugarli

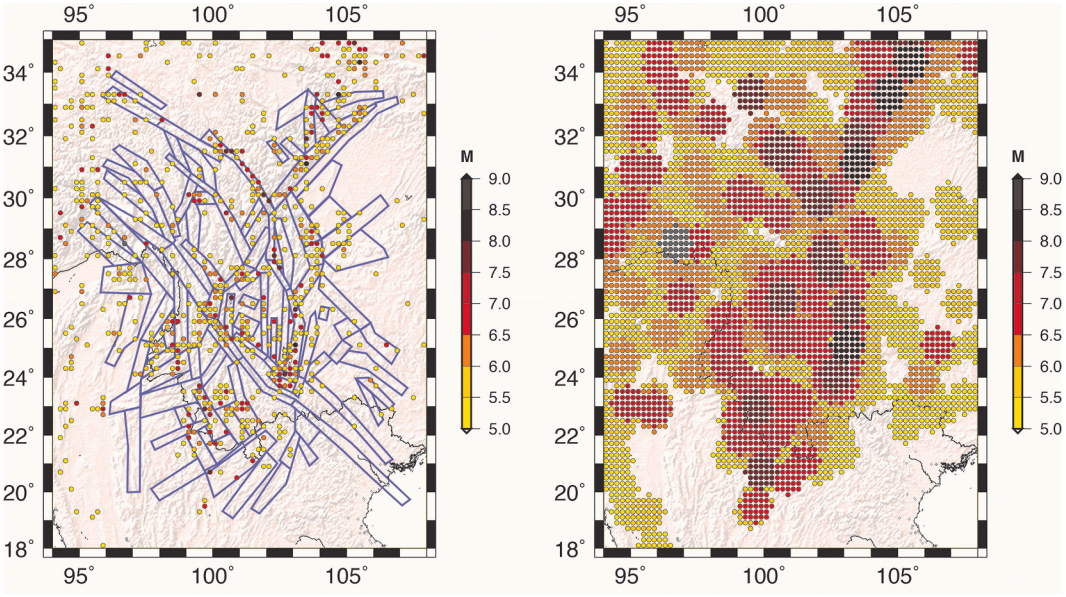

Fig. 6. Left: Spatial distribution of the 99 seismogenic zones and gridded seismicity with 0.2° × 0.2° cells from CSESeventV2020; Right: Spatial distribution of historical and instrumental seismicity smoothed with the radius of 3 cells (Panza et al., 1996) from CSESeventV2020.

et al., 2019b). The same Authors defined:

$$M_{design} = M_{max} + \gamma_{EM}\sigma_M$$

where the magnitude of MCE is obtained by summing to the maximum observed or estimated magnitude ($M_{\max}$) the product of the global standard deviation σ_M and a safety factor γ_{EM}. In CSES case, if considering $\gamma_{EM} = 2.0$ and $\sigma_M = 1/4$ (Båth, 1973; Panza and Bela, 2020), we get $\gamma_{EM}\sigma_M = 0.5$. Gorshkov et al. (2003) defined a series of earthquake-prone segments (nodes) prone to $M \geq 8.2$ in the transasian seismic belt outside its Alpine zone. Nine of these seismogenic nodes are within the present study area (Fig. 7 [left]). Considering $M_{\max} = 8.2$, i.e., the magnitude threshold given by Gorshkov et al. (2003), the upper bound estimates in all nine nodes is $M_{\text{design}} = 8.7$ (Fig. 7 [right]). The radius of each circle depends on a threshold magnitude M (in this case, $M = 8.2$). When considering the largest earthquake ($M \geq 8.2$), its size is typically 100 – 300 km (Gorshkov et al., 2003). And therefore, we defined $R = 100$ km (thus diameter = 200 km) as a conservative value of radius in depicting the circles of seismogenic nodes. The effect of $R = 150$ km (thus diameter = 300 km), as a more conservative parametric test, was also computed. The results demonstrate that the increment of radius from 100 km to 150 km did not significantly change the results of the hazard computations when R = 100 km (see Section 3 of Supplementary Material). The representative focal mechanism of each seismogenic node was defined in two ways: (1) using the focal mechanism defined in the seismogenic zone including the node, and (2) using the focal mechanism defined in the nearest seismogenic zone to the node in the case of no seismogenic zone covering the node. The computations of realistic synthetic seismograms were made considering all the sources within seismogenic zones and nodes (Fig. 8).

3.4. Focal mechanisms

According to the rules of NDSHA (Rugarli et al., 2019a and references therein; http://www.xeris.it/Hazard/), at least one focal mechanism is supposed to be defined in a seismogenic zone, and the defined focal mechanism must be representative of the characteristic seismotectonics in corresponding seismogenic zone. In general, if one polygon describing a seismogenic zone includes more than one mechanism, a representative focal mechanism (earthquake source tensor) will be computed by averaging the tensors' properties. For each seismogenic zone, Mourabit et al. (2014) defined the focal mechanism of the largest event falling in the seismogenic zone as a representative focal mechanism and assigned a representative focal mechanism compatible with the tectonic regime and geology of the zone without available information. Parvez et al. (2017) adopted a more complex and articulated strategy to equip seismogenic zones with their characteristic focal mechanisms: (a) the strongest events, (b) the best studied event, (c) the most frequent event and (d) the average focal mechanisms computed from available moment tensor solutions. Indeed, it is not easy or practical to identify "*the best studied*" and "*the most frequent*" in literatures, but the strongest event can be, as a rule, found easily.

In 2019, the CSES released community models consisting of the first-generation unified velocity model, fault model, strain model, relocation earthquake catalogue and focal mechanisms catalogue.[6] The focal mechanisms catalogue (2009 – 2017)[1] provides a direct way to define representative focal plane solutions for seismogenic zones (Fig. 5). To prepare more options for defining the characteristic focal mechanism for each seismogenic zone, the GCMT results from 1976 to 2008 were also considered.[7] The strategy followed here to equip each seismogenic zone with its characteristic focal mechanism can be schematized as follows: (1) giving priority to the focal mechanisms catalogue released in 2019, (2) for the seismogenic zones without focal plane solutions defined in (1), using available GCMT results, and (3) for the seismogenic zones without any fault plane solutions defined in (1) and (2), the reported nearest focal mechanisms were used. Cui et al. (2005) studied the characteristics of focal mechanisms in China and adjacent areas. They found that the focal mechanisms in the areas adjacent to the Tibetan region mainly represent strike-slip and normal types, which provides enough confidence for our definition to focal mechanisms in 99 seismogenic zones (Fig. 5).

3.5. Structural models

In the past 50 years, significant progresses regarding the physical knowledge of Earth's structure, particularly the mechanical properties of

[6] http://www.ief.ac.cn/Community/index.html. Last accessed on April 30, 2020.

[7] https://www.globalcmt.org/. Last accessed on January 20, 2021.

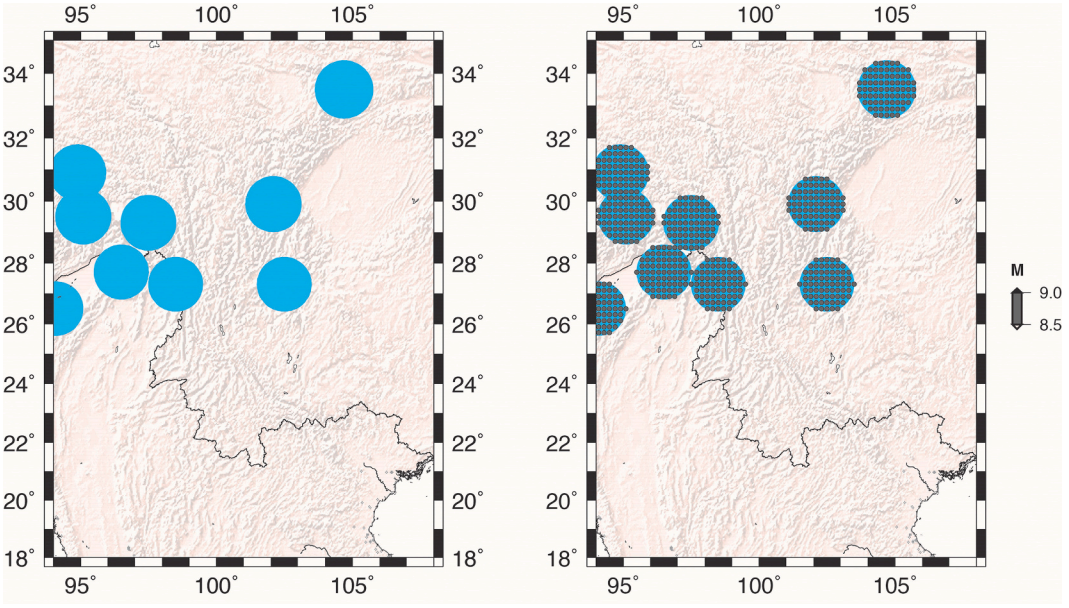

Fig. 7. Left: Spatial distribution of nine seismogenic nodes (cyan circles, Radius = 100 km) prone to large earthquakes with $M \geq 8.2$ identified by Gorshkov et al. (2003). Right: Sources inside seismogenic nodes. (For interpretation of the references to colour in this figure legend, the reader is referred to the web version of this article.)

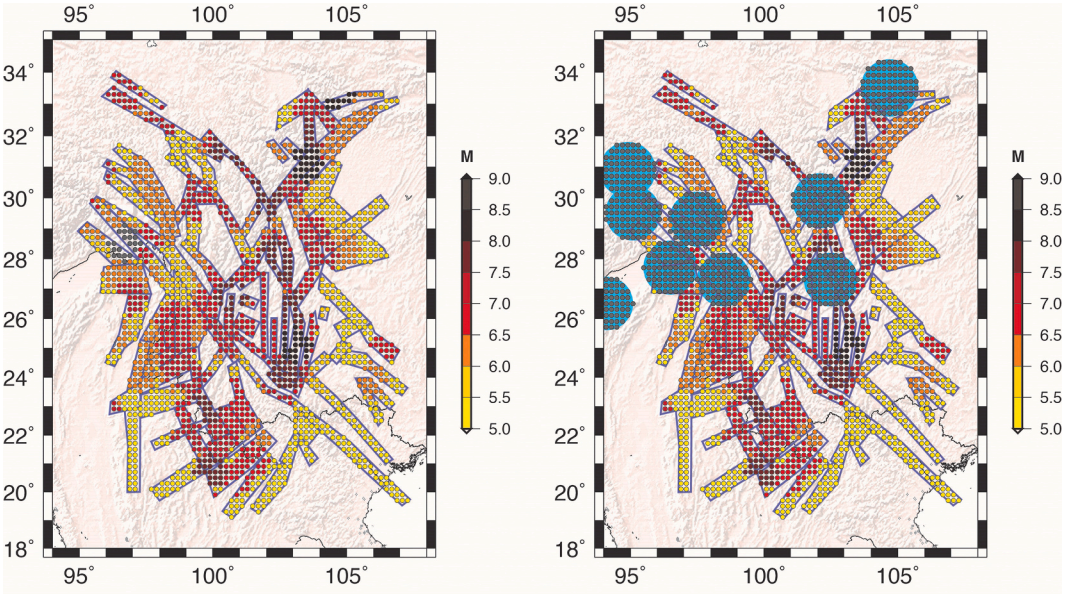

Fig. 8. Left: Graphic representation of "smoothed" seismicity in each seismogenic zone. Right: Graphic representation of "smoothed" seismicity in each seismogenic zone and nodes.

the crust and upper mantle, have been obtained because of the improvement of detection accuracy. One progress was the establishment of the global models, such as PREM (Dziewonski and Anderson, 1981), IASP91 (Kennett and Engdahl, 1991), SP6 (Morelli and Dziewonski, 1993), AK135 (Kennett et al., 1995), CRUST5.1 (Mooney et al., 1998), and CRUST1.0 (Laske et al., 2013). However, global average structural models only describe approximate information regarding the crust and upper mantle in large scale. More detailed structural models are essential for computing reliable and realistic seismograms in the NDSHA framework.

Based on non-linear surface wave tomography, suitable structural properties at a regional scale have been defined by Zhang et al. (2014) by means of 2° × 2° cellular structural models of the lithosphere-asthenosphere system beneath the Qinghai-Tibet Plateau and adjacent areas. Yao et al. (2019) built a 3D velocity model based on the joint linearized inversion of Rayleigh wave dispersion, ZH ratio and receiver function (Zhang and Yao, 2017). Zhang et al. (2014) and Yao et al. (2019) provided two choices for defining the structural models in our study area. It is difficult to determine which model (or bedrock condition) is better. Accordingly, we defined two different models to be considered as input: (1) Model A, directly taken from the results of Zhang et al. (2014); (2) Model B, a combination of the results of Zhang et al. (2014) and Yao et al. (2019). In Model A, we considered the 2° × 2° cellular structural models defined by Zhang et al. (2014). As shown in Fig. 9, 56 cells reaching nearly 350 km in depth were assembled according to Zhang et al. (2014). In particular, for cells 53, 54, 55, and 56,

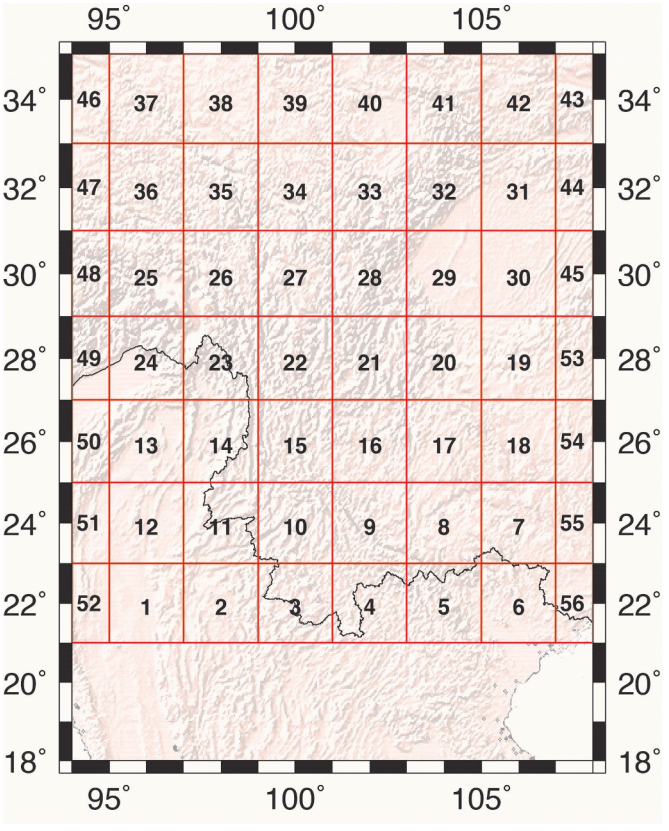

Fig. 9. The 2° × 2° cellular grid identifying cellular structural models. At the east and west edges of the study area, the cells from 43 to 56 are 1° × 2°.

the structural models were assembled using their adjacent cells, i.e., cells 19, 18, 7, and 6. For each cellular structural model, as in Zhang et al. (2014), the uppermost four layers (32 km) were fixed and the layered velocity models down to approximately 350 km of depth were taken from the results of Zhang et al. (2014). The empirical relationship between the quality factor, *Qs*, and shear wave velocity, Vs, proposed by Olsen et al. (2003) was considered in each unit, as stated in Eq. (1):

$$Q_s = 100V_s \tag{1}$$

The general relationship between *Qs* and *Qp* was used in (2).

$$Q_p = \frac{9}{4}Q_s \tag{2}$$

Model B was obtained by replacing, in the depth range of 0 – 80 km, the layered structures of Model A with the results of Yao et al. (2019). Finally, all structural models in Models A and B were extended to a depth of 1100 km using AK135-F (Montagner and Kennett, 1996). Three examples of *Vp*-velocity, Vs-velocity and density vertical profiles, for the cellular models cse0012, cse0021 and cse0036 in Models A and B, are shown in Figs. 10 and 11.

4. Computations

In general, from the perspective of reliable modelling techniques of seismic wavefields, three aspects of the physical processes must be taken into account, i.e., the earthquake source process, propagation pathways and local site effects (Panza, 2017). In our computations, the size scaled point source (SSPS) approximation was firstly adopted (Gusev, 1983). In terms of propagation pathways, because we were interested mostly in peak values of ground motion parameters, an approximate but robust way to deal with the effect of lateral heterogeneities was to assume the structural model at the site of interest as the representative model of the whole propagation pathways of seismic waves (Panza et al., 2001).To minimize the effect of the uppermost layers (i.e., local soil effect) and of high-frequency attenuation in the near field, an upper frequency of 1 Hz was considered. Such upper frequency bound is sufficient to include main parts of seismic wavetrains at a regional scale (Panza et al., 2001; Panza et al., 2012).

In the procedure of computing synthetic seismograms, some conventions and/or assumptions were set to optimize the computation. For all selected cells, magnitudes were grouped into three levels, i.e., $M<7$, $7 \le M < 8$, $M \ge 8$, and hypocentral depth (h_d) was regarded as a function of the value of magnitude. For $M < 7$, h_d was set at 10 km, for $7 \le M < 8$,

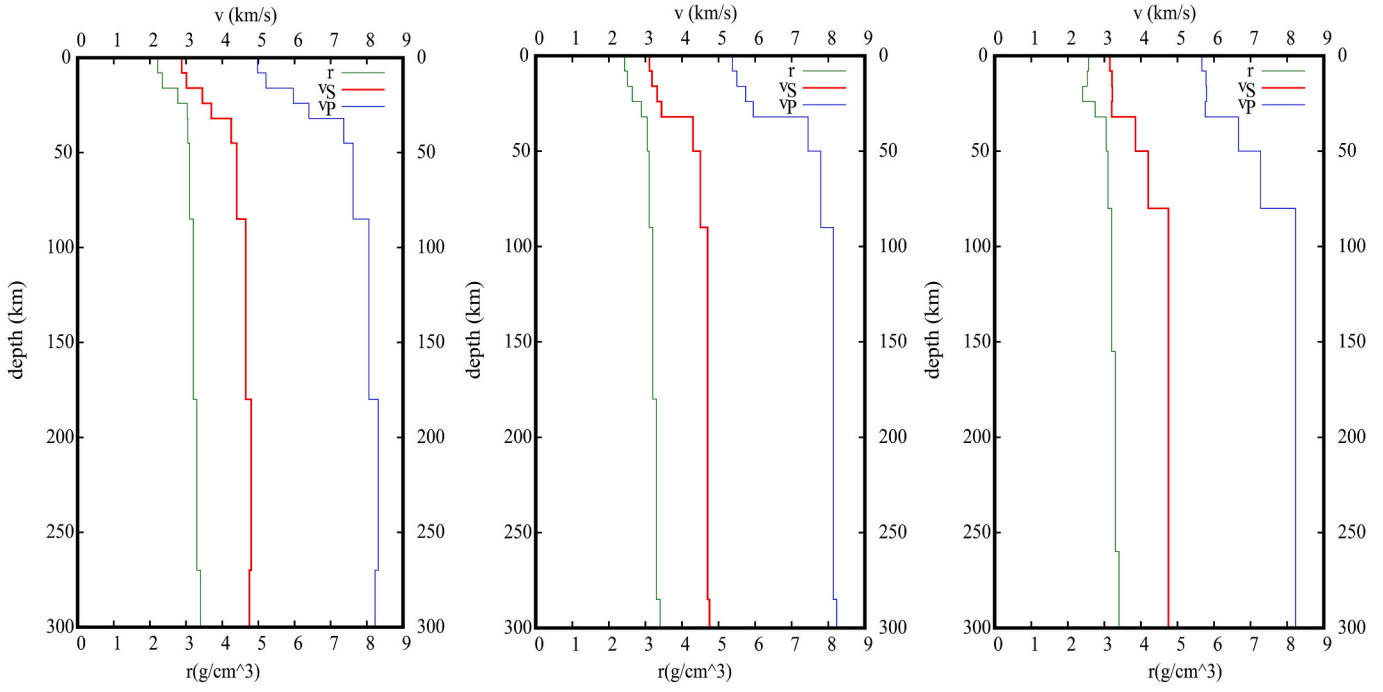

Fig. 10. Examples of V_p-velocity, V_s-velocity and density vertical profiles, for the cellular models cse0012, cse0021 and cse0036 in Model A.

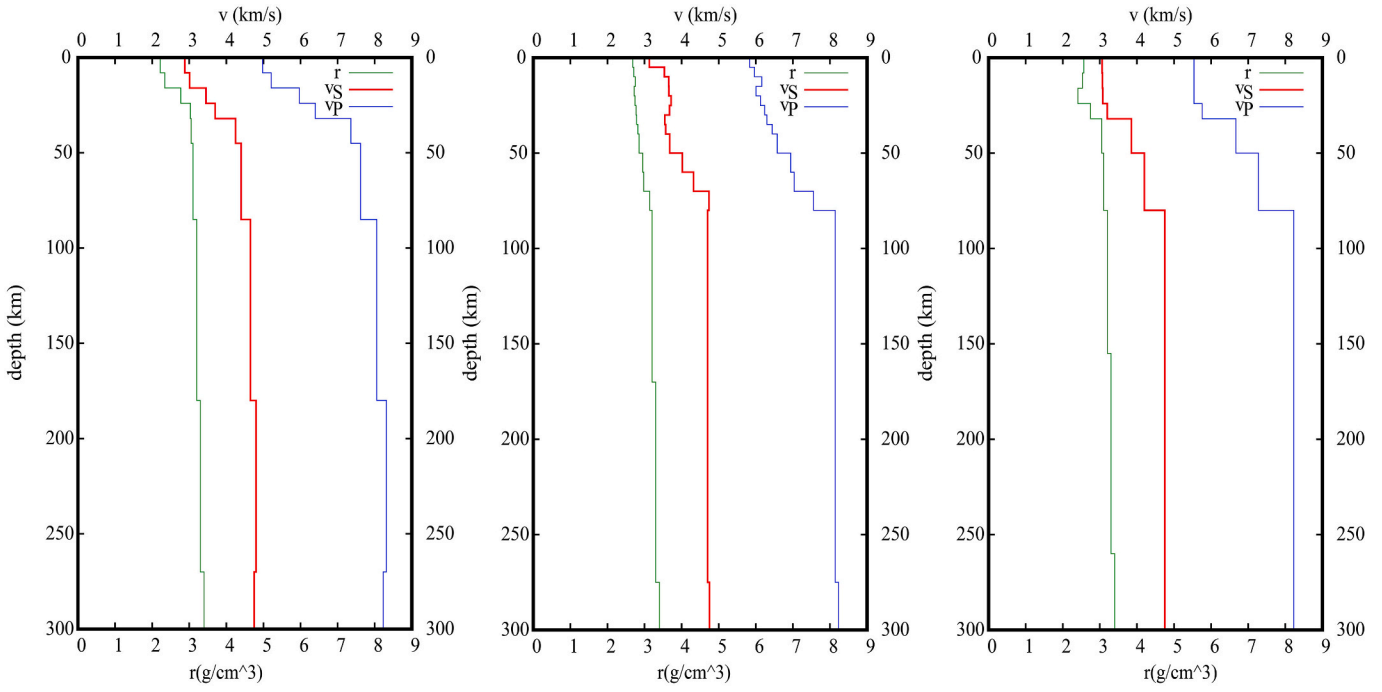

Fig. 11. Examples of V_p-velocity, V_s-velocity and density vertical profiles, for the cellular models cse0012, cse0021 and cse0036 in Model B.

h_d was set at 15 km, and for $M \geq 8$, h_d was set at 25 km. To reduce the number of computed synthetic seismograms, without losing important information, the maximum source-site distance was set, as a rule, at 150 km. The peak ground motion parameters could be readily extracted from the computed synthetic seismograms. However, the executive frequency of 1 Hz cannot represent dominant parts of acceleration time series or spectra (e.g., Panza et al., 1997). Accordingly, a design response spectrum adopted in "designs of structures for earthquake resilience" was used to extrapolate NDSHA acceleration to higher frequency. Here, the normalized elastic acceleration response spectra Eurocode-8 (EC8) for soil type "A" (e.g., Eurcode-8, 2004), i.e., hard soil on the topmost structural layer with $V_s > 0.8$ km/s (bedrock condition), and 5% critical damping, was considered to obtain the value of DGA, i.e., design ground acceleration (Panza et al., 2001; Panza and Bela, 2020). DGA is obtained by two steps: (a) computing synthetic accelerograms at long-period portion ($T > 1$ s), and (b) by matching the long-period portion of the normalized spectra (i.e., design response spectra) with modelled synthetic accelerograms, the value of absolute spectrum could be obtained at $T = 0$ s, and is defined as DGA. Although DGA is obtained by extrapolation, the adopted method for extrapolation (i.e., normalized spectra, EC8) basically considers the soil type. Actually, to use the response spectra of recordings of real events having similar magnitudes/distances to those of synthetic seismograms computed for the study area is very promising; however, it is more appropriate on specific earthquake scenarios, while this paper is more focused on the methodology on seismic hazard assessment at a regional scale.

Geophysical scientists are skilful at modelling (or predicting) future potential events based on past records (Kossobokov et al., 2015). In order to test the predictive power of NDSHA, all events after the occurrence of May 12th, 2008 $M_s = 8.0$ Wenchuan earthquake (including itself) were removed in the assembled catalogue CSESeventV2020. It provided the opportunity to temporarily go back to the time point before the occurrence of this damaging earthquake and perform independent NDSHA computations. The comparison of hazard computations before/after the Great Wenchuan event reasonably measured stability and predictive power of hazard computations of NDSHA.

5. Results

Two groups of computations, at 1 Hz cut-off frequency, were performed considering Models A and B in the study area. The two structural models only differ in the depth range of 0 – 80 km and are identical for larger depths. Consequently, a comparison of the results obtained with Models A and B, even if they both belong to the bedrock conditions, allowed us to identify the influence from variations in bedrock. Such kind of variations are fully neglected in standard PSHA. A detailed analysis of 3D effects, based on modal summation (La Mura et al., 2011; Gholami et al., 2014), to identify relevant local effects due to variations in bedrock conditions is the subject of a forthcoming paper.

Here, the results considering CSESeventV2020 and seismogenic nodes associated with M_{design} ($\gamma_{EM} \neq 0$) (see Section 2 of Supplementary Material) were used to discuss the hazard level in the study area. As showed in Figs. 12, 13, and 14, PGD, PGV and DGA values start to decrease and remain at a low level close to the east boundary of the study area, in reasonable relation to the eastern stable South China Block. The PGD maps (Fig. 12) demonstrate that the areas with PGD values in the range of 30 – 60 cm are mostly distributed along the Longmenshan, Xianshuihe, Anninghe, Zemuhe, Xiaojiang, Honghe, and Lijiang-Xiaojinhe Fault Zones, the EHS and its surrounding areas. In the adjacent areas, the PGD values can be as high as 15 cm. The PGV maps (Fig. 13) demonstrate that the areas with PGV values in the range of 60 – 120 cm/s are somehow mimicking fault (zones) and mainly focus on the Zemuhe, Daliangshan, and northeastern Longmenshan Fault Zones, and the EHS. The PGV values in the most of the study area exceed 8 cm/s. The DGA maps (Fig. 14) show high hazardous areas along Xiaojiang Fault Zone, central segment of Honghe Fault Zone, Lijiang-Xiaojinhe Fault Zone, northern and southern segments of Xianshuihe Fault Zone, Longmenshan Fault Zone and the EHS, where DGA values can exceed 0.6 g. The DGA values in the most of the study area are not less than 0.08 g; in other words, the potential macroseismic intensity I_{MM}(Wald et al., 1999) is greater than VII (Fig. 15). The strongest instrumental acceleration recorded at the occurrence of the May 12th, 2008 $M_s = 8.0$ Wenchuan earthquake was 0.96 g (i.e., the value of 957.7 gal, recorded at a strong-motion seismometer deployed in Wolong town, Wenchuan County) reported by Yu et al. (2008). We can observe that the magnitude

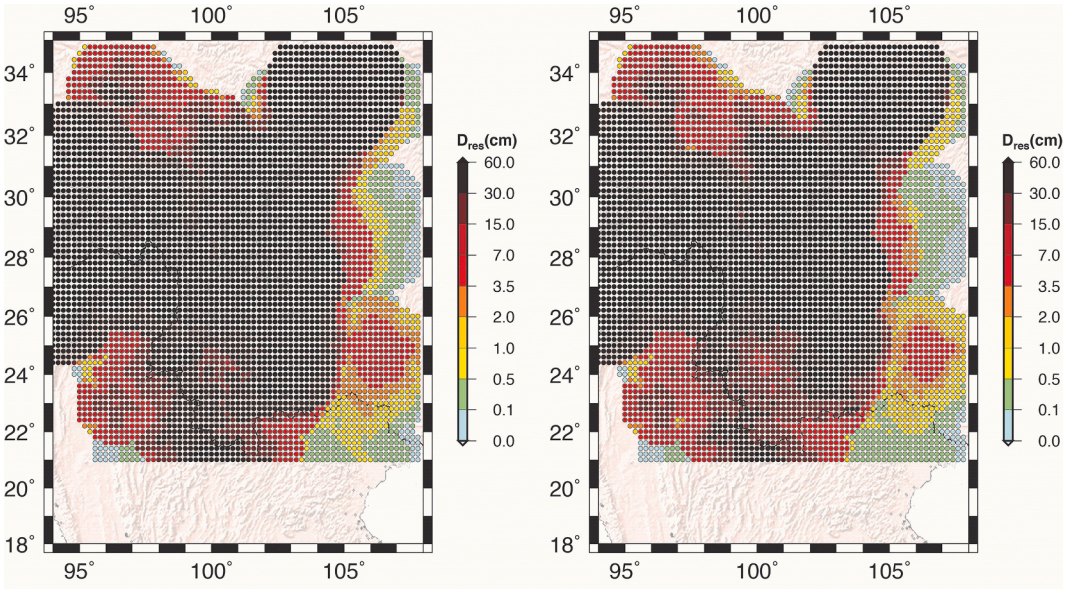

Fig. 12. Computed peak ground displacement (PGD) map considering CSESeventV2020 and seismogenic nodes associated with $M_{\text{design}}(\gamma_{\text{EM}} \neq 0)$ (Left: Using Model A; Right: Using Model B).

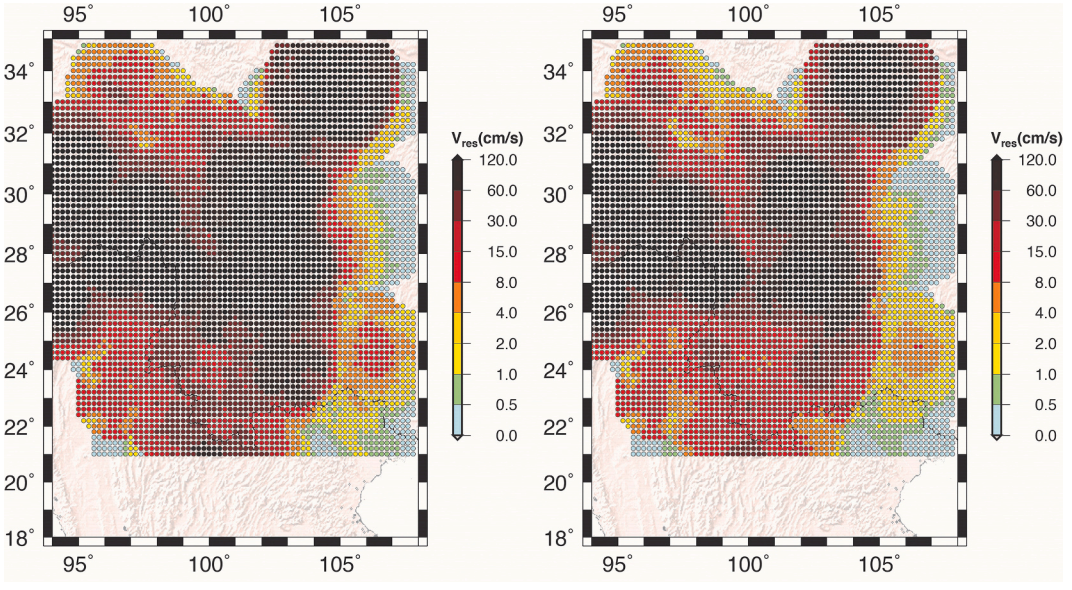

Fig. 13. Computed peak ground velocity (PGV) map considering CSESeventV2020 and seismogenic nodes associated with $M_{\text{design}}(\gamma_{\text{EM}} \neq 0)$. (Left: Using Model A; Right: Using Model B).

of the May 12$^{\text{th}}$, 2008 M_s = 8.0 Wenchuan earthquake did not necessarily reach that of the Maximum Credible Earthquake (MCE) defined in Section 3.3. In 2013, a M_s = 7.0 earthquake struck Lushan County in Yaan City, Sichuan Province. For the first time, a PGA value larger than 1.0 g was recorded in China (Wen et al., 2013). The DGA maps (Fig. 14) demonstrate DGA values around Lushan are as high as 1.2 g. Therefore, such a value is not a surprise for NDSHA. Therefore, the NDSHA estimation is in a good agreement with the peak ground motion value recorded in actual field observation. The probabilistic seismic hazard map of China, as reported by NSGMP (GB18306 – 2015),[8] shows the maximum PGA value is 0.4 g with 10% probability of exceedance in 50 years, and the PGA values in the most areas of the Sichuan and Yunnan Provinces are 0.15 g with 10% probability of exceedance in 50 years.

On the other hand, it is impossible to include all historical events in the selected study area. We have performed additional computations to estimate how much the two strong events (1920 December 16$^{\text{th}}$, 1920 M_s = 8.5 Haiyuan earthquake and May 23$^{\text{rd}}$,1927 M_s = 8.0 Gulang earthquake) that occurred 200 – 300 km to the north boundary of the study area could affect the results of the hazard estimation in the study area (see Section 1 in Supplementary Material). We also tested the influence of the introduction of seismogenic nodes by comparing the results after/before inserting them and tested the influence of γ_{EM} by comparing the results obtained with $\gamma_{EM} \neq 0$ and $\gamma_{EM} = 0$ (see Section 2 in Supplementary Material). The results show that computations made considering parametric catalogue CSESeventV2020 and seismogenic nodes substantially remedy the defects caused by the natural incompleteness in the assembled catalogue CSESeventV2020. The hazard

[8] http://www.gb18306.net/. Last accessed on March 9, 2021.

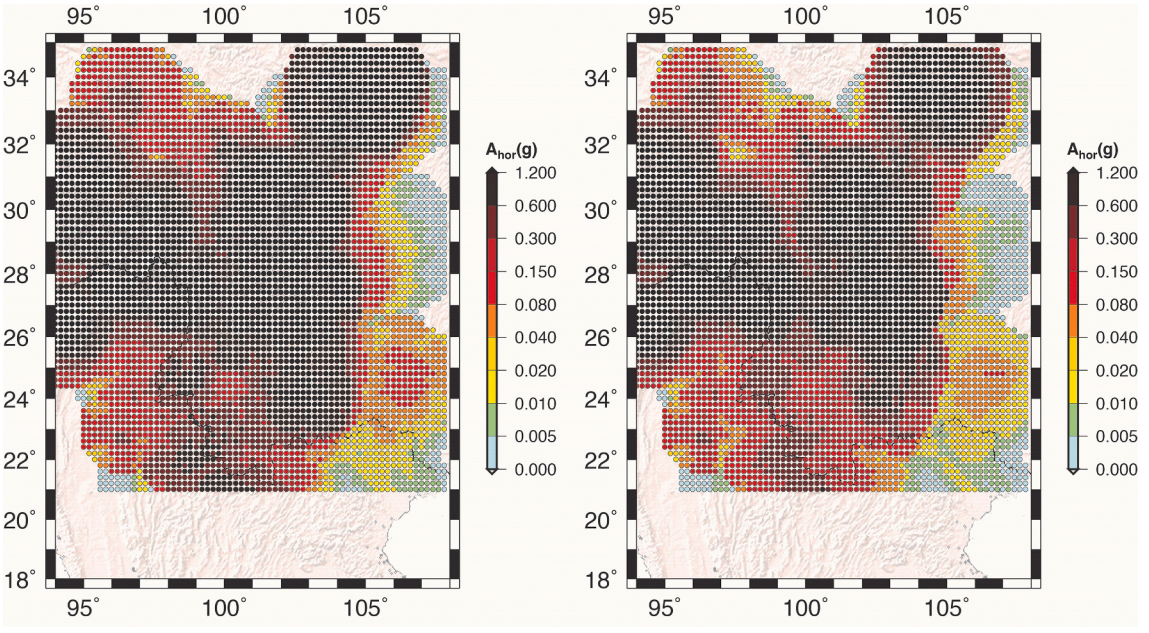

Fig. 14. Computed design ground acceleration (DGA) map considering CSESeventV2020 and seismogenic nodes associated with $M_{\text{design}}(\gamma_{\text{EM}} \neq 0)$. (Left: Using Model A; Right: Using Model B).

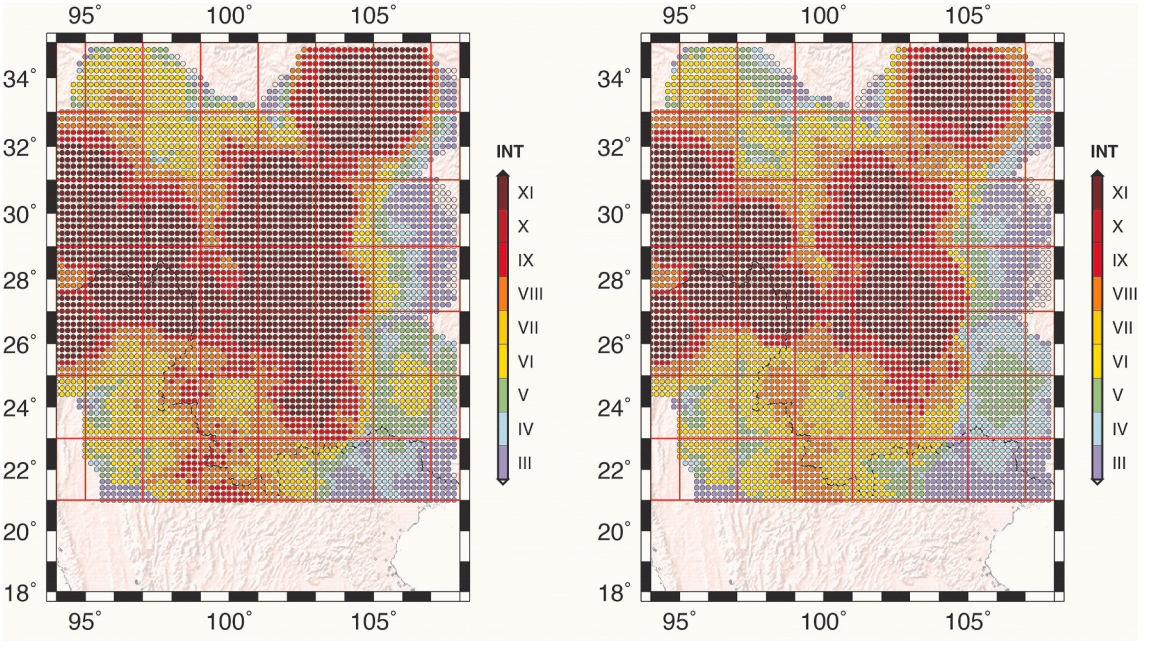

Fig. 15. Macroseismic intensity map using the conversion relations between I_{MM} and peak ground acceleration proposed by Wald et al. (1999). (Left: Using Model A; Right: Using Model B).

results we computed with $\gamma_{EM} \neq 0$ added to the threshold magnitude (8.2) are consistent with the Maximum Credible Earthquake (MCE) (Rugarli et al., 2019b), which supply a more comprehensive description to seismic hazard in the CSES area.

As previously mentioned, the predictive power of NDSHA could be tested by removing the May 12$^{\text{th}}$, 2008 $M_s = 8.0$ Wenchuan earthquake and all its subsequent events (also called stability tests). Two tentative computations were performed to test the predictive power of NDSHA: (1) only considering CSESeventV2020 (removing the Great Wenchuan event and all its subsequent events), and (2) considering CSESeventV2020 (removing the Great Wenchuan event and all its subsequent events) and seismogenic nodes associated with M_{design} ($\gamma_{EM} \neq 0$). The results are shown in Figs. S26-S28 in Supplementary Material. Here, what we were interested in presenting is not the seismic hazard level before May 12$^{\text{th}}$, 2008 $M_s = 8.0$ Wenchuan earthquake, but the common and different features of computed DGA maps before/after that damaging earthquake. As shown in Fig. 16, the DGA values computed before the Great Wenchuan earthquake remain the same in most of the areas, compared with the values computed with the full CSESeventV2020, and differences mainly exist in the northwest and southwest parts of the study area.

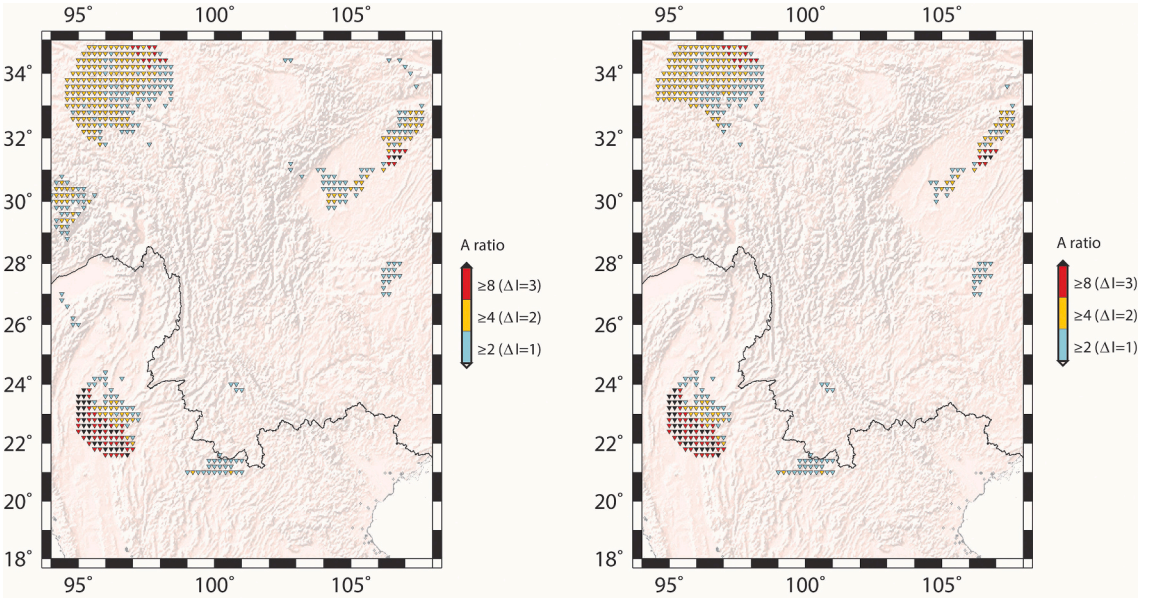

Fig. 16. Ratios between the design ground accelerations computed from the computations before/after the May 12th, 2008 M_s = 8.0 Wenchuan Event. Left: Only considering assembled catalogue CSESeventV2020; Right: Considering CSESeventV2020 and seismogenic nodes associated with $M_{design}(\gamma_{EM} \neq 0)$. The downward triangles indicate that the DGA values before the May 12th, 2008 M_s = 8.0 Wenchuan Event are smaller than the DGA values computed after that event.

6. Model validation

Actually, it is inappropriate to be concerned about mice when there are tigers abroad (Box, 1976). In order to look for tigers and calibrate what we have modelled so far, the May 12th, 2008 M_s = 8.0 Wenchuan earthquake occurred in the Longmenshan Fault Zone was selected as the scenario event for model validation. The modelled peak ground motions were compared with available strong ground motion data recorded around the epicenter, within a distance of 500 km. Here, we directly used the information of May 12th, 2008 M_s = 8.0 Wenchuan event recorded in the assembled catalogue CSESeventV2020, i.e., epicenter at 103.4°E, 31.0°N, M_s = 8.0. The focal mechanism was taken from the definition provided in Section 3.4 (Focal Mechanisms), i.e., Strike = 221°, Dip = 31° and Rake = 61°. We chose as focal depth value the one corresponding, for the standard regional computations, to the events with $M \geq$8.0, i.e., 25 km. Then, as a sort of simple parametric study, we considered also a focal depth value of 20 km, in agreement, within experimental errors, with the ones reported in literature (14–20 km, e.g., Liu et al., 2008) and to the one that we adopted for events with 7.0 $\leq M <$ 8.0, in agreement with some literature, e.g., Caputo et al. (1973), Molchan et al. (1997) and Doglioni et al. (2015). In the following step we have performed parametric tests similar to those made by Rastgoo et al. (2018), who modelled the June 20th, 1990 M_w = 7.4 Manjil-Rudbar (Iran) earthquake, and focal depth varied within acceptable uncertainties. In the two computations (h_d = 20 km, 25 km), the source model remained as SSPS model (Gusev, 1983), the results of which are shown in Fig. 17. Using the relationships between peak ground accelerations and Modified Mercalli Intensity (MMI) proposed by Wald et al. (1999), we obtained the distribution of intensity (MMI) from Fig. 17. The results are shown in Fig. 18. Li et al. (2010) obtained a simple

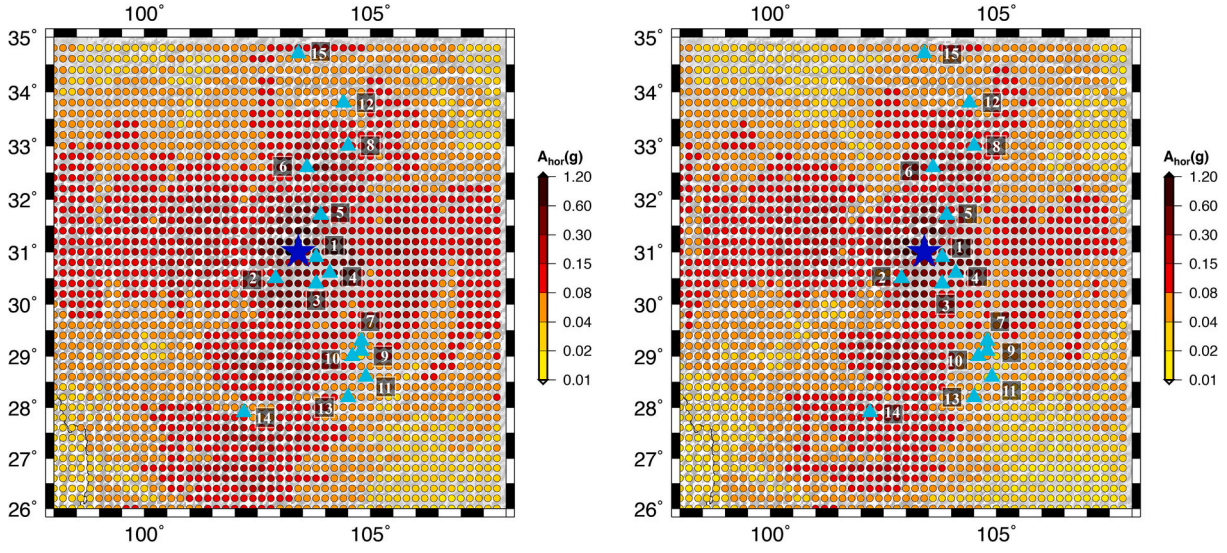

Fig. 17. Results of two modelling computations for the May 12th, 2008 M_s = 8.0 Wenchuan earthquake based on the SSPS earthquake source model. Blue star: epicenter; triangles labeled with white number: accelerometric stations. Left: focal depth defined at 20 km; Right: Focal depth defined at 25 km. (For interpretation of the references to colour in this figure legend, the reader is referred to the web version of this article.)

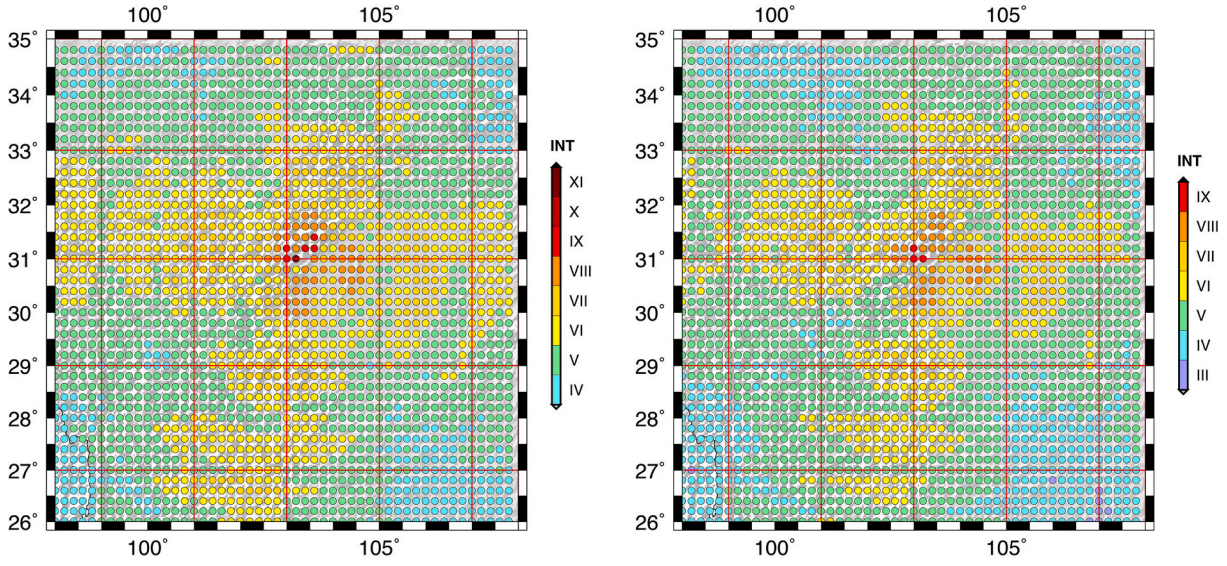

Fig. 18. Macroseismic intensity map obtained from Fig. 17 using the conversion relationships between Modified Mercalli Intensity and peak ground acceleration proposed by Wald et al. (1999). Left: focal depth defined at 20 km; Right: Focal depth defined at 25 km.

distribution of MMI Intensities by computing co-seismic displacement based on the assumed parameters (including location, magnitude, depth, and faulting mechanisms) of May 12th, 2008 $M_s = 8.0$ Wenchuan earthquake. When comparing the modelled intensity distribution (Fig. 18) with intensity maps computed by Li et al. (2010) and USGS,[9] the coverage of high intensity areas $I \geq IX_{MMI}$ differs, but the pattern of $I = VI_{MMI}$ areas are similar in the northeast-southwest direction. Worthy to note, the fault mechanism and parameters (including the seismic intensity distribution) of the May 12th, 2008 $M_s = 8.0$ Wenchuan event have been discussed and updated in later publications since 2008 (e.g., Lekkas, 2010; Yang et al., 2011), meaning that one could have a variety of choices for the selection of a benchmark. However, in general, the purpose of modelling is not to be in total agreement with all existing results, but basically to match the main features. The resulting macroseismic intensity map of the May 12th, 2008 $M_s = 8.0$ Wenchuan earthquake by Li et al. (2010) and USGS may not be the most representative, but both of them depicted basic features of macroseismic intensity distribution of that event.

In order to evaluate and validate the results of hazard computation, we selected the accelerometric stations (bedrock condition) located at the epicentral distance of 0 – 500 km for comparison with the modelled results. The criteria above are satisfied by 15 stations, which are basically distributed around the epicenter (Fig. 17). The details of 15 stations and modelled DGA bands are listed in Table 1. At each selected site, the estimated DGA bands (i.e., error range) were considered in the comparison (Fig. 19). The agreement between the modelled DGA values and observed values indicates the absence of tigers and the presence of mice. In more detail, at the fifth (51MXT, PGA: 0.43 g, DGA band: 0.15 – 0.30 g) and the eighth site (62WIX, PGA: 0.201 g, DGA band: 0.08 –0.15 g), the observed PGA values are +0.130 g (43%) and + 0.051 g (34%) larger than the maximum of estimated DGA bands. That may mean that local detailed investigations are necessary around these two stations, whose records can contain effects due to currently unknown local site properties. At the same time, the disagreement at sites 51MXT and 62WIX indicates the necessity to consider rupture process for detailed modelling. In the PGV case, the observed PGV values recorded at the two same stations (51MXT and 62WIX) are +0.185 m/s (123%) and + 0.082 m/s (103%) larger than the maximum of estimated PGV bands (see Fig. S29 in Supplementary Material). In the map of NSGMP, the PGA values at 51MXT and 62WIX are 0.2 g with 10 probability of exceedance in 50 years. In addition, at the other 13 sites, the estimated DGA bands are not exceeded by recorded PGA values. Worthy to note, the change trends of DGA bands and recorded PGA values are corelated, especially in the epicentral range of 50 – 100 km and 200 – 250 km. And it is not difficult to observe the similar agreement in PGA and PGV comparison of Lushan case (see Fig. S30 and S31 in Supplementary Material). Therefore, the actual observations successfully validated our modelling results.

Based on the results described above, the reliability of the seismic hazard estimation in the framework of NDSHA is supported by four reasons: (1) The modelling processes are based on physical knowledge about seismic sources and propagation ray-paths. (2) The use of seismogenic nodes deals, to some extent, with the potential incompleteness of parametric historical catalogues. (3) From the DGA map computed using the parametric catalogue CSESeventV2020 (see Fig. S13 in Supplementary Material), one could find that the estimated DGA range in the Longmenshan Fault Zone is 0.6 – 1.2 g, which covers the maximum acceleration recorded for the 2008 $M_s = 8.0$ Wenchuan earthquake, i.e., 0.96 g (Yu et al., 2008). (4) The comparison performed at 15 sites (on bedrock condition) between the observed records and the results of regional NDSHA computation (bedrock condition), considering the seismicity before the 2008 $M_s = 8.0$ Wenchuan earthquake (see Fig. S28 in Supplementary Material), shows that all observed records are enveloped by the estimated DGA band by NDSHA (Fig. 20).

7. Discussion

In order to proceed with the deterministic seismic hazard analysis in the area of CSES, we collected and updated all the necessary datasets for the study area, including the focal mechanisms, CSESeventV2020, the seismogenic zones, nodes and structural models (Model A and Model B). Naturally, e.g., due to the observation level and physical knowledge limitations, these datasets have limited abilities in describing the seismological and geophysical features of such a large and tectonically complex study area. Accordingly, the limitations and uncertainties are unavoidable in any seismic hazard assessment analyses.

It is worth mentioning that seismogenic nodes, as a supplement to the parametric catalogue CSESeventV2020, have been used to obtain a conservative hazard estimation, effectively managing the intrinsic

[9] https://earthquake.usgs.gov/earthquakes/eventpage/usp000g650/shakemap/intensity. Last accessed on August 31, 2020.

Table 1
Resultant of horizontal PGA components (NS & EW) obtained from records in the accelerometric stations (bedrock condition) deployed around the epicenter of the May 12th, 2008 $M_s = 8.0$ Wenchuan earthquake and computed DGA from NDSHA scenario computations (focal depth = 20 km; 25 km).

SN	SN*&SL	SC	ED	PGA	Focal Depth: 20 km		Focal Depth: 25 km	
					Class	DGA	Class	DGA
1	51PXZ (103.8, 30.9)	R	39.733	0.186	0.3 – 0.6	0.392	0.15 – 0.3	0.238
2	51BXZ (102.9, 30.5)	R	73.308	0.193	0.15 – 0.3	0.201	0.15 – 0.3	0.212
3	51XJL (103.8, 30.4)	R	76.901	0.14	0.08 – 0.15	0.145	0.15 – 0.3	0.156
4	51CDZ (104.1, 30.6)	R	80.301	0.106	0.3 – 0.6	0.311	0.3 – 0.6	0.315
5	51MXT (103.9, 31.7)	R	91.175	0.43	0.15 – 0.3	0.26	0.15 – 0.3	0.212
6	51SPT (103.6, 32.6)	R	178.913	0.05	0.3 – 0.6	0.302	0.15 – 0.3	0.229
7	514ZG (104.8, 29.3)	R	232.057	0.041	0.04 – 0.08	0.06	0.04 – 0.08	0.046
8	62WIX (104.5, 33)	R	245.386	0.201	0.08 – 0.15	0.124	0.08 – 0.15	0.12
9	51FSB (104.8, 29.1)	R	250.577	0.04	0.04 – 0.08	0.041	0.04 – 0.08	0.045
10	51YBY (104.6, 29)	R	250.615	0.049	0.04 – 0.08	0.05	0.04 – 0.08	0.046
11	51CNT (104.9, 28.6)	R	303.58	0.023	0.04 – 0.08	0.054	0.02 – 0.04	0.037
12	62ZHQ (104.4, 33.8)	R	325.187	0.05	0.04 – 0.08	0.078	0.04 – 0.08	0.05
13	51JLT (104.5, 28.2)	R	329.002	0.021	0.04 – 0.08	0.075	0.04 – 0.08	0.044
14	51XCX (102.2, 27.9)	R	363.751	0.007	0.04 – 0.08	0.069	0.08 – 0.15	0.114
15	62LTA (103.4, 34.7)	R	411.421	0.013	0.04 – 0.08	0.067	0.04 – 0.08	0.066

SN, Station Number; SN*, Station Name; SL, Station Location; SC, Site Condition; R, Rock.
ED, Epicentral Distance, unit: km.
PGA, Peak Ground Acceleration, unit: g; DGA, Design Ground Acceleration, unit: g.

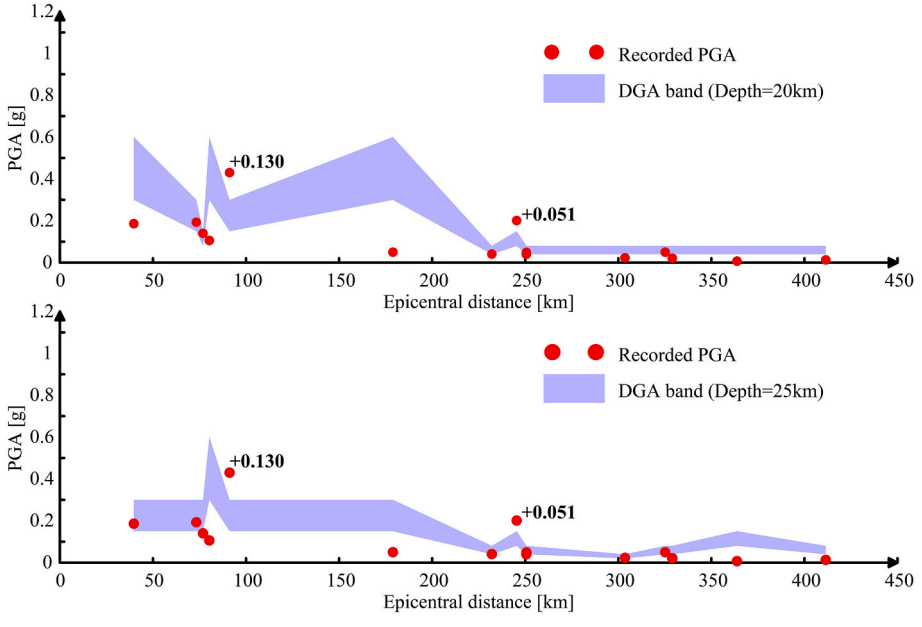

Fig. 19. Scatter plots, marked by red circles, of recorded PGA (resultant values from NS and EW component) at 15 sites in rock condition and corresponding estimated DGA range (Top panel: focal depth = 20 km; Bottom panel: focal depth = 25 km) versus epicentral distance considering the scenario, May 12th, $M_s = 8.0$ Wenchuan earthquake. The narrow bands colored by light blue indicate the error of modelled DGA values. The range is determined considering standard discrete ranges of DGA hazard values as determined for MCS scale by Panza and Bela (2020). For example, a DGA value of 0.55 g, is assigned to the range 0.30 – 0.60 g. At the fifth station (i.e., 51MXT, see Table 1), the observed PGA value is 0.130 g (43%) larger than the maximum of modelled DGA band (0.15 – 0.30 g); at the eighth station (i.e., 62WIX, see Table 1), the observed PGA value is 0.051 g (34%) larger than the maximum of modelled DGA band (0.08 – 0.15 g). (For interpretation of the references to colour in this figure legend, the reader is referred to the web version of this article.)

incompleteness of any parametric earthquake catalogue. In fact, the definition of M_{design} is considered as an envelope (i.e., the upper-limit value) of Maximum Credible Earthquake (MCE) evaluated at the basis of present-day formalized knowledges. Should the magnitude of new earthquakes exceed, within standard errors, M_{design} values, by means of the formalized procedures defined by NDSHA it is possible to readily update seismic hazard maps with an acceptable CPU time effort. For example, a complete standard hazard computation in the CSES area takes about 25 h using a 2.26 GHz CPU.

Stability of results and negligible influence of two large events (i.e., the 1920, December 16th $M_s = 8.5$Haiyuan and 1927, May 23th $M_s = 8.0$ Gulang earthquakes) located outside the study area were also verified.

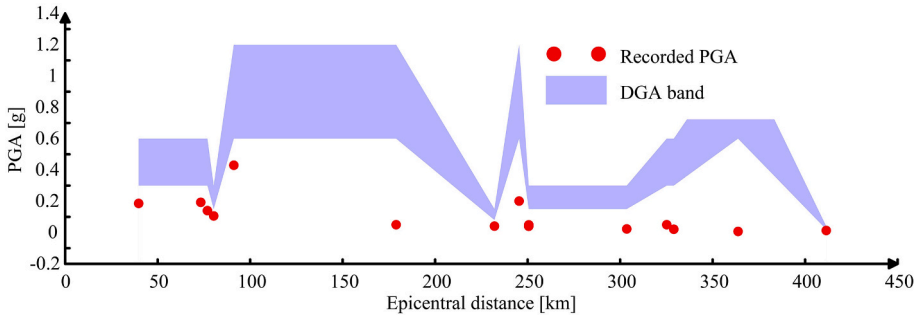

Fig. 20. Scatter plots, marked by red circles, of recorded PGA (resultant values from NS and EW component) at 15 sites in bedrock conditions and corresponding estimated DGA ranges defined by the NDSHA computation only considering the seismicity before the occurrence of May 12th, 2008 $M_s = 8.0$ Wenchuan earthquake versus epicentral distance. (For interpretation of the references to colour in this figure legend, the reader is referred to the web version of this article.)

(1) Stability: by removing the Great Wenchuan Event (and all its subsequent events), we were able to test the predictive power of NDSHA computations, and further to see the stability of the results. The comparisons shown in Fig. 16 illustrate that the adoption of the truncated catalogue is able to portray the main seismic activity in the study area. The newly added records after the occurrence of the Great 2008 $M_s = 8.0$ Wenchuan event (i.e., the full catalogue CSESeventV2020) change the distribution of peak ground parameters (PGD, PGV, and DGA) within an acceptable error range ($\Delta I \leq 2$, i.e., two Intensity degrees). This validates the stability of seismic hazard level assessment in the study area and of the results of the NDSHA computations. (2) Large events located outside the study area: the results obtained from the additional analysis of their effects on the hazard assessment suggest that it is reasonable to ignore their influence, at least for standard settlements. In fact, an in-depth analysis of their possible effects on long period ground motion may be appropriate when considering the application of seismic isolation techniques (e.g., Martelli and Forni, 2010; Martelli et al., 2014), a practice which is very diffused in China (e.g., Zhou, 2001; Pan et al., 2012), and could be the subject of future studies.

8. Conclusions

In this work, we performed regional neodeterministic (physics-based) seismic hazard assessment in the study area containing the Sichuan-Yunnan region and the Southeast margin of Tibetan Plateau. For the computation of synthetic seismograms, we collected the required datasets, including earthquake catalogues, seismogenic zones and nodes, focal mechanisms, and structural models, in a form suitable for earthquake hazard computation. Stability tests have been performed and the negligible influence from large magnitude events located "far" from the study area has been verified. The obtained seismic hazard maps are described by the spatial distribution of PGD, PGV and DGA values, extracted from synthetic seismograms computed at a regional scale and mapped on a regular grid of $0.2^\circ \times 0.2^\circ$. Primary conclusions are listed below:

(1) Stability tests indicate that seismic hazard computations are basically not impacted by a reasonable variation of the input parametric catalogue, supporting the long-term effectiveness of the obtained hazard maps and the predictive power of NDSHA.
(2) The comparisons between observed peak ground motions and results of scenario computations of 2008, May 12th $M_s = 8.0$, Great Wenchuan earthquake and 2013, April 20th $M_s = 7.0$, Lushan earthquake at a regional scale (bedrock condition) show a reasonable correlation.
(3) The tests performed for estimating the potential influence from large events outside the study area (i.e., the 1920, December 16th $M_s = 8.5$, Haiyuan and 1927, May 23rd $M_s = 8.0$, Gulang earthquakes) show that the estimated hazard values are not much impacted by them.
(4) The insertion of seismogenic nodes makes up the intrinsic incompleteness of the earthquake catalogue, and makes it possible to readily update the seismic hazard maps once the defined M_{design} is exceeded.

The main results show that the DGA values could reach 0.6 g around main faults and/or fault zones, including Longmenshan, Xianshuihe, Anninghe, Zemuhe, Xiaojiang and Honghe Fault Zones, indicating that high seismic hazard is a significant feature of the region.

For the seismically active Sichuan and Yunnan Provinces, these maps represent not only the first attempt to estimate seismic hazard with a neodeterministic, physics-based, approach, but they also provide a new reference choice for structural engineers and decision makers. In fact, these first order seismic zoning results can be used to update regional disaster mitigation actions, and provide the foundations for two items potentially important in the near future: (1) application of the neodeterministic approach to other important areas, e.g., Northwest China, Northeast China, and South China; (2) start multi-scenario urban-scale researches (or site- specific SHA) in the most hazardous areas pointed out in the study region. Moreover, these first-order zoning NDSHA findings may serve as a knowledge basis to support both large- to mid-spatial (i.e., the whole mainland China and North China) and time (i.e., from the Two Centenary Goals[10] to the 14th Five-Year Plan[11]) range preparedness actions, like the improvement and reinforcement of the infrastructures with different designed life, and to (multi-scenario) site-specific studies.

Data availability

The information about the Seismic Ground Motion Parameters Zonation Map of China can be found at http://www.gb18306.cn/, where we got the seismogenic zones used in this paper. The detailed longitude and latitude information about seismogenic nodes were provided by Vladimir G. Kossobokov (personal communication) from Institute of Earthquake Prediction and Mathematical Geophysics, Russian Academy of Sciences. The focal mechanisms catalogues used in this paper can be found at http://www.ief.ac.cn/Community/info/2020/22555.html and GCMT (https://www.globalcmt.org/). The catalogue CSESeventV2020 was assembled from two parts, the old catalogue before 1990, which could be found in *The Catalogue of Chinese Historical Strong Earthquakes* (in Chinese) (1995) and *The Catalogue of Chinese Modern Earthquakes* (in Chinese) (1999); the new catalogue from 1990 to

[10] http://www.china.org.cn/china/china_key_words/2014-11/18/content_34158771.htm. Last accessed on May 3, 2021.
[11] http://en.qstheory.cn/The14thFiveYearPlan.html. Last accessed on May 3, 2021.

2019 was obtained from China Earthquake Networks Center (CENC). The partial information about the velocity model used in this paper can be found in http://www.ief.ac.cn/Community/info/2020/22540.html. The strong ground motion data were provided by China Strong Motion Network Centre at Institute of Engineering Mechanics, China Earthquake Administration.

Funding

The work was supported by the Special Fund of China Seismic Experimental Site [grant number: 2019CSES0101].

Declaration of Competing Interest

The authors declare that they have no known competing financial interests or personal relationships that could have appeared to influence the work reported in this paper.

Acknowledgements

We are grateful to the Editor and two anonymous Reviewers for their constructive comments and recommendations, which helped us to significantly improve the manuscript and better clarify our points. We like to express our sincere appreciation to China Seismic Experimental Site (CSES), Institute of Earthquake Forecasting, China Earthquake Administration (IGP, CEA) and Department of Mathematics and Geosciences, University of Trieste (DMG, UNITS). We express our thanks to the Compiling Committee of the Seismic Ground Motion Parameters Zonation Map of China for providing the potential seismogenic zones, to the China Earthquake Networks Center (CENC) for providing earthquake catalogues since 1970, to the Department of Earthquake Disaster Prevention, China Earthquake Administration for providing earthquake catalogues before 1990, to the China Strong Motion Network Centre at Institute of Engineering Mechanics, and the China Earthquake Administration for providing strong ground motion data. This work was mainly accomplished during the special period of COVID-19 pandemic in the world. The authors would like to express their great respect and gratitude to all the medical workers around the world who have worked so hard to fight the virus. The first author wants to express his special thanks to Mr. Xiao Yong and Dr. Li Jiawei for helping download and transmit the ground motion data, to Dr. Kou Huadong and Dr. Tan Youheng for meaningful discussion about velocity models and seismic sources, and to Dr. Nie jihua for her help in studying in Trieste. Last but not least, the first author expresses his the most special thanks to Miss Yuan Yushuang for her trust, support and understanding during the period when he was studying in Trieste, Italy.

Appendix A. Supplementary data

Supplementary data to this article can be found online at https://doi.org/10.1016/j.enggeo.2021.106208.

References

Båth, M., 1973. Introduction to Seismology. Birkhäuser, Basel.

Bela, J., Panza, G.F., 2021. NDSHA – the new paradigm for RSHA – an updated review. Vietnam J. Earth Sci. 43, 111–188.

Box, G.E.P., 1976. Science and statistics. J. Am. Stat. Assoc. 71, 791–799.

Caputo, M., Keilis-Borok, V., Kronrod, T., Molchan, G., Panza, G.F., Piva, A., Podgaetskaja, V., Postpischl, D., 1973. Models of earthquake occurrence and isoseismals in Italy. Ann. Geofis. 26, 421–444.

Chen, Y., David, C.B., 2011. The Wenchuan Earthquake of 2008: Anatomy of a Disaster. Springer-Verlag.

Chen, Y.X., Liu, M., Luo, G., 2020. Complex temporal patterns of large earthquake: devils' staircase. Bull. Seismol. Soc. Am. 110, 1064–1076.

Cheng, J., Rong, Y., Magistrale, H., Chen, G., Xu, X., 2017. An -based historical earthquake catalogue for mainland China. Bull. Seismol. Soc. Am. 107, 2490–2500.

Cornell, C.A., 1968. Engineering seismic risk analysis. Bull. Seismol. Soc. Am. 58, 1583–1606.

Cui, X.F., Xie, F.R., Zhao, J.T., 2005. The regional characteristics of focal mechanisms solutions in China and its adjacent areas. Seismol. Geol. 27, 298–307 (In Chinese with English abstract).

Deng, Q.D., Zhang, P.Z., Ran, Y.K., Yang, X.P., Min, W., Chen, L.C., 2003. Active tectonics and earthquake activities in China. Earthquake Sci. Front. 10 (S1), 66–73.

Department of Earthquake Disaster Prevention, China Earthquake Administration, 1999. The Catalogue of Chinese Modern Earthquakes. China Science and Technology Press (in Chinese with English abstract).

Department of Earthquake Disaster Prevention, State Seismological Bureau, 1995. The Catalogue of Chinese Historical Strong Earthquakes. Seismological Press (in Chinese with English abstract).

Ding, Z.F., Vaccari, F., Chen, Y.T., Panza, G.F., 2004. Deterministic seismic hazard map in North China. In: Chen, Y.T., Panza, F.G., Wu, Z.L. (Eds.), Earthquake Hazard, Risk, and Strong Ground Motion. Seismological Press, pp. 351–360.

Doglioni, C., Carminati, E., Petricca, P., Riguzzi, F., 2015. Normal fault earthquakes or graviquakes. Sci. Rep. 5 (12110),1–12.

Dziewonski, A.M., Anderson, D.L., 1981. Preliminary reference earth model. Phys. Earth Planet. Inter. 25, 297–356.

El-Sayed, A., Vaccari, F., Panza, G.F., 2001. Deterministic seismic hazard in Egypt. Geophys. J. Int. 144, 555–567.

Eurocode-8, 2004. Design of structures for earthquake resistance, Part 1: General rules, seismic actions and rules for buildings. In: Authority: The European Union Per Regulation 305/2011, Directive 98/34/EC, Directive 2004/18/EC.

Florsch, N., Fäh, D., Suhadolc, P., Panza, G.F., 1991. Complete synthetic seismograms for high-frequency multimode SH-waves. Pure Appl. Geophys. 136, 529–560.

Gan, W.J., Zhang, P.Z., Shen, Z.K., Niu, Z.J., Wang, M., Wan, Y.G., Zhou, D.M., Cheng, J., 2007. Present-day crustal motion within the Tibetan Plateau inferred from GPS measurements. J. Geophys. Res. 112, B08416.

Gao, M.T., Tian, B., 2015. GB 18306–2015 Chinese Seismic Zonation Map: Publicizing Materials (Chinese Edition). Standard Press of China (in Chinese).

Gholami, V., Hamzehloo, H., La Mura, C., Ghayamghamian, M.R., Panza, G.F., 2014. Simulation of selected strong motion records of the 2003 M_W=6.6 Bam earthquake (SE Iran), the modal summation-ray tracing methods in the WKBJ approximation. Geophys. J. Int. 196, 1–15.

Gorshkov, A., Kossobokov, V., Soloviev, A., 2003. Recognition of earthquake-prone areas. In: Vladimir, K.B., Soloviev, A.A. (Eds.), Nonlinear Dynamics of the Lithosphere and Earthquake Prediction. Springer-Verlag, pp. 239–310.

Gusev, A.A., 1983. Descriptive statistical model of earthquake source radiation and its application to an estimation of short-period strong motion. Geophys. J. Int. 74, 787–808.

Gvishiani, A.D., Soloviev, A.A., Dzeboev, B.A., 2020. Problem of recognition of strong-earthquake-prone areas: a state-of-the-art review. Izvestiya. Phys. Soild Earth 56, 1–23.

Kennett, B.L.N., Engdahl, E.R., 1991. Travel times for global earthquake location and phase association. Geophys. J. Int. 105, 429–465.

Kennett, B.L.N., Engdahl, E.R., Buland, R., 1995. Constraints on seismic velocities in the Earth from traveltimes. Geophys. J. Int. 122, 108–124.

Kossobokov, V.G., Peresan, A., Panza, G.F., 2015. Reality check: seismic hazard models you can trust. Eos 96, 9–11.

Kron, W., 2002. Keynote lecture: flood risk= hazard× exposure× vulnerability. Flood Defence 82–97.

La Mura, C., Yanovskaya, T.B., Romanelli, F., Panza, G.F., 2011. Three-dimensional seismic wave propagation by modal summation: method and validation. Pure Appl. Geophys. 168, 201–216.

Laske, G., Masters, G., Ma, Z., Pasyanos, M., 2013. Update on CRUST1.0 – A 1-degree global model of Earth's crust. Geophys. Res. Abstr. 15, 2658.

Lekkas, E.L., 2010. The 12 May 2008 Mw7.9 Wenchuan, China, earthquake: macroseismic intensity assessment using the EMS-98 and ESI 2007 Scales and their correlation with the geological structure. Bull. Seismol. Soc. Am. 100 (5B), 2791–2804.

Li, W.D., Zhang, C.J., Li, D.H., He, J.Y., Chen, H.Z., Cinna, L., 2010. Early estimate of epicenter seismic intensities according to co-seismic deformation. Geofis. Int. 49, 107–112.

Liu, Q.Y., Chen, J.H., Li, S.C., Li, Y., Guo, B., Wang, J., Qi, S.H., 2008. The M_S8.0 Wenchuan earthquake: preliminary results from the Western Sichuan mobile seismic array observations. Seismol. Geol. 30, 584–596.

Liu, R.F., Chen, Y.T., Xue, F., 2017. The measured magnitude should not be converted to each other. Seismol. Geomagnet. Observ. Res. 39, 3 (in Chinese with English Abstract).

Markušić, S., Sunadolc, Herak, M., Vaccari, F., 2000. A contribution to seismic hazard. Assessment in Croatia from deterministic modeling. Pure Appl. Geophys. 157, 185–204.

Martelli, A., Clemente, P., De Stefano, A., Forni, M., Salvatori, A., 2014. Recent development and application of seismic isolation and energy dissipation and conditions for their correct use. In: Ansal, A. (Ed.), Perspectives on European Earthquake Engineering and Seismology. Springer International Publishing, pp. 449–488.

Martelli, A., Forni, M., 2010. Seismic isolation and other antiseismic systems: recent applications in Italy and worldwide. Seismic Isolat. Protect. Syst. 1, 75–123.

McGuire, R.K., 2008. Probabilistic seismic hazard analysis: early history. Earthq. Eng. Struct. Dyn. 37, 329–338.

Molchan, G., Kronrod, T., Panza, G.F., 1997. Multi-scale seismicity model for seismic risk. Bull. Seismol. Soc. Am. 87, 1220–1229.

Montagner, J.P., Kennett, B.L.N., 1996. How to reconcile body-wave and normal-mode reference earth models. Geophys. J. Int. 125, 229–248.

Mooney, W.D., Laske, G., Masters, G., 1998. CRUST 5.1: A global crustal model at 5° × 5°. J. Geophys. Res. Soild Earth 103, 727–747.
Morelli, A., Dziewonski, A.M., 1993. Body ware traveltimes and a spherically symmetric P- and S- wave velocity model. Geophys. J. Int. 112, 178–194.
Mourabit, T., Abou Elenean, K.M., Ayadi, A., et al., 2014. Neo-deterministic seismic hazard assessment in North Africa. J. Seismol. 18, 301–318.
Olsen, K.B., Day, S.M., Bradley, C.R., 2003. Estimation of Q for long-period (> 2 sec) waves in the Los Angeles Basin. Bull. Seismol. Soc. Am. 93, 627–638.
Pan, P., Ye, L.P., Shi, W., Cao, H.Y., 2012. Engineering practice of seismic isolation and energy dissipation structures in China. SCIENCE CHINA Technol. Sci. 55, 3036–3046.
Pan, H., Gao, M.T., Xie, F.R., 2013. The earthquake activity model and seismicity parameters in the New Seismic Hazard Map of China. Technol. Earthquake Disast. Prevent. 8, 11–23 (in Chinese with English abstract).
Panza, G.F., 1985. Synthetic seismograms: the Rayleigh waves modal summation. J. Geophys. 58, 125–145.
Panza, G.F., 2017. NDSHA: Robust and Reliable Seismic Hazard Assessment arXiv preprint arXiv:1709.02945.
Panza, G.F., Bela, J., 2020. NDSHA: a new paradigm for reliable seismic hazard assessment. Eng. Geol. 275, 105403.
Panza, G.F., Prozorov, A., Suhadolc, P., 1990. Is there a correlation between lithosphere structure and statistical properties of seismicity? In: Cassinis, R., Panza, G.F. (Eds.), The Structure of the Alpine - Mediterranean Area: Contribution of Geophysical Methods, Terra Nova, vol. 2, pp. 585–595.
Panza, G.F., Vaccari, F., Costa, G., Suhadolc, P., Fäh, D., 1996. Seismic input modelling for zoning and microzoning. Earthquake Spectra 12, 529–566.
Panza, G.F., Cazzaro, R., Vaccari, F., 1997. Correlation between macroseismic intensities and seismic ground motion parameters. Annali di Geofisica XL 5, 1371–1382.
Panza, G.F., Romanelli, F., Vaccari, F., 2001. Seismic wave propagation in laterally. Heterogeneous anelastic media: theory and application to seismic zonation. Adv. Geophys. 43, 1–95.
Panza, G.F., La Mura, C., Peresan, A., Romanelli, F., Vaccari, F., 2012. Seismic hazard scenarios as preventive tools for a disaster resilient society. Adv. Geophys. 53, 93–165.
Panza, G.F., Peresan, A., La Mura, C., Committee, U.E.J., 2013. Seismic hazard and strong ground motion: an operational neo-deterministic approach from national to local scale. In: Encyclopedia of Life Support Systems (EOLSS), Geophysics and Geochemistry, Developed under the Auspices of the UNESCO, pp. 1–49.
Parvez, I.A., Vaccari, F., Panza, G.F., 2003. A deterministic seismic hazard map of India and. Adjacent areas. Geophys. J. Int. 155, 489–508.
Parvez, I.A., Magrin, A., Vaccari, F., et al., 2017. Neo-deterministic seismic hazard scenarios for India – a preventive tool for disaster mitigation. J. Seismol. 21, 1559–1575.
Peresan, A., Ogwari, O.P., 2010. Preliminary compilation of a unified earthquake catalogue for North Africa. In: The Abdus Salam International Centre for Theoretical Physics, ICTP. Trieste, Internal Report IC/IR/2010/004.
Peresan, A., Zuccolo, E., Vaccari, F., Gorshkov, A., Panza, G.F., 2011. Neo-deterministic seismic hazard and pattern techniques: Time-dependent scenarios for North-Eastern Italy. Pure Appl. Geophys. 168, 583–607.
Rastgoo, M., Rahimi, H., Romanelli, F., Vaccari, F., Panza, F.G., 2018. Neo-deterministic seismic hazard assessment for Alborz Region, Iran. Eng. Geol. 242, 70–80.
Rugarli, P., Amadio, C., Peresan, A., Fasan, M., Vaccari, F., Magrin, A., Romanelli, F., Panza, G.F., 2019a. Neo-deterministic scenario-earthquake accelerograms and spectra: A NDSHA approach to seismic analysis. In: Jia, J.B., Paik, J.K. (Eds.), Engineering Dynamics and Vibrations: Recent developments. CRC Press, pp. 187–241.
Rugarli, P., Vaccari, F., Panza, G.F., 2019b. Seismogenic nodes as a viable alternative to seismogenic zones and observed seismicity for the definition of seismic hazard at regional scale. Vietnam J. Earth Sci. 41, 289–304.
Sarica, G.M., Zhu, T., Pan, T.C., 2020. Spatio-temporal dynamics in seismic exposure of Asian megacities: past, present and future. Environ. Res. Lett. 15, 094092.
Shen, Z.K., Lü, J.N., Wang, M., Bürgmann, R., 2005. Contemporary crustal deformation around the southeast borderland of the Tibetan Plateau. J. Geophys. Res. 110, B11409.
Stirling, M.W., 2014. The continued utility of probabilistic seismic hazard assessment. In: Wyss, M., Shroder, J. (Eds.), Earthquake Hazard, Risk, and Disasters. Elsevier, pp. 359–376.
Vaccari, F., El Qadi, A., Ramdani, M., Ait, B.L., Limouri, M., Tadil, B., 2001. Deterministic seismic hazard assessment for North Morocco. J. Seismol. Earthquake Eng. 3, 1–12.
Wald, D.J., Quitoriano, V., Heaton, H.T., Kanamori, H., 1999. Relations between peak ground acceleration, peak ground velocity and Modified Mercalli Intensity in California. Earthquake Spectra 15, 557–564.
Wang, P., Shao, Z.G., Liu, Q., Wei, W.X., Yin, X.F., 2019. Probabilistic forecasting of earthquakes based on. Multidisciplinary physical observations and its application in Sichuan and Yunnan. Chin. J. Geophys. 62, 3448–3463 (In Chinese with English abstract).
Wen, X.Z., Ma, S.L., Xu, X.W., He, Y.N., 2008. Historical pattern and behavior of earthquake ruptures. Along the eastern boundary of the Sichuan-Yunnan faulted-block, southwestern China. Phys. Earth Planet. Inter. 168, 16–36.
Wen, R.Z., Ren, Y.F., Qi, W.H., Lu, T., Yang, Z.Y., Shan, Z.D., Wang, Y.L., 2013. Maximum. Acceleration recording from Lushan earthquake on April, 2013. J. Southwest Jiaotong Univ. 48, 783–791 (In Chinese with English abstract).
Wu, J.D., Wang, C.L., He, X., Wang, X., Li, N., 2017. Spatiotemporal changes in both asset value and GDP associated with seismic exposure in China in the context of rapid economic growth from 1990 to 2010. Environ. Res. Lett. 12, 034002.
Wu, Z.L., Zhang, Y., Li, J.W., 2019. Coordinated distributed experiments (CDEs). Applied to earthquake forecast test sites. In: Li, Y.G. (Ed.), Earthquake and Disaster Risk: Decade Retrospective of the Wenchuan Earthquake. Springer, pp. 107–115.
Wyss, M., Nekrasova, A., Kossobokov, V., 2012. Errors in expected human losses due to incorrect seismic hazard estimates. Nat. Hazards 62, 927–935.
Xu, W.J., Gao, M.T., 2014. Statistical analysis of the completeness of earthquake catalogues in China mainland. Chin. J. Geophys. 57, 2802–2812 (in Chinese with English abstract).
Yang, X.L., Wu, Z.L., Jiang, C.S., Xia, M., 2011. Estimating intensities and/or strong motion parameters using civilian monitoring videos: the May 12, 2008, Wenchuan earthquake. Pure Appl. Geophys. 168, 753–766.
Yang, S.B., Qiao, Y.S., Wu, Z.H., Zhang, X.J., Qi, L., He, Z.X., Liang, Y., 2020. Paleoearthquake investigation along the Chenghai Fault Zone since ~500ka, Southeast Margin of the Tibetan Plateau. J. Geol. Soc. China. https://doi.org/10.1111/1755-6724.14513.
Yao, H.J., Yang, Y., Wu, M.X., Zhang, P., Wang, M.M., 2019. Crustal shear velocity model in southeast China from joint seismological inversion. In: CSES Scientific Products. https://doi.org/10.12093/02md.02.2018.01.v1.
Yu, H.Y., Wang, D., Yang, Y.Q., Lu, D.W., Xie, Q.C., Zhang, M.Y., Zhou, B.F., Jiang, W.X., Cheng, X., Yang, J., 2008. The preliminary analysis of strong ground motion characteristics from the Ms 8.0 Wenchuan Eartquake, China. J. Eng. Eng. Vibr. 3, 321–336 (In Chinese with English abstract).
Zhang, P., Yao, H.J., 2017. Stepwise joint inversion of surface wave dispersion, Rayleigh wave ZH ratio, and receiver function data for 1D crustal shear wave velocity structure. Earthq. Sci. 30, 229–238.
Zhang, P.Z., Deng, Q.D., Zhang, G.M., Ma, J., Gan, W.J., Min, W., Mao, F.Y., Wang, Qi, 2003. Active tectonic blocks and strong earthquakes in the continent of China. Sci. China Ser. D Earth Sci. 46, 13–24.
Zhang, P.Z., Wen, X.Z., Xu, X.W., Gan, W.J., Wang, M., Shen, Z.K., Wang, Q.L., Huang, Y., Zheng, Y., Li, X.J., Zhang, Z.Q., Ma, S.L., Ran, Y.K., Liu, Q.Y., Ding, Z.F., Wu, J.P., 2009. Tectonic model of the great Wenchuan earthquake of May 12, 2008, Sichuan, China. Chin. Sci. Bull. 54, 944–953 (in Chinese).
Zhang, X.M., Teng, J.W., Sun, R.M., Romanelli, F., Zhang, Z.J., Panza, G.F., 2014. Structural model of the lithosphere-asthenosphere system beneath the Qinghai-Tibet Plateau and its adjacent areas. Tectonophysics 634, 208–226.
Zhou, F.L., 2001. Seismic isolation of civil buildings in the People's Republic of China. Prog. Struct. Eng. Mater. 3, 268–276.